Validity and limitations of the superexchange model for the magnetic properties of Sr_2IrO_4 and Ba_2IrO_4 mediated by the strong spin-orbit coupling

I. V. Solovyev,[1,2,*] V. V. Mazurenko,[2] and A. A. Katanin[3,2]

[1]*Computational Materials Science Unit, National Institute for Materials Science, 1-1 Namiki, Tsukuba, Ibaraki 305-0044, Japan*

[2]*Department of Theoretical Physics and Applied Mathematics, Ural Federal University, Mira str. 19, 620002 Ekaterinburg, Russia*

[3]*Institute of Metal Physics, S. Kovalevskoy Str. 18, 620990 Ekaterinburg, Russia*

(Received 27 August 2015; revised manuscript received 1 November 2015; published 7 December 2015)

Layered perovskites Sr_2IrO_4 and Ba_2IrO_4 are regarded as the key materials for understanding the properties of magnetic relativistic insulators, mediated by the strong spin-orbit (SO) coupling. One of the most fundamental issues is to which extent these properties can be described by the superexchange (SE) model, formulated in the limit of the large Coulomb repulsion for some appropriately selected pseudospin states, and whether these materials themselves can be classified as Mott insulators. In this work, we address these issues by deriving the relevant models and extracting parameters of these models from the electronic-structure calculations with the SO coupling, based on the density functional theory. First, we construct the effective Hubbard-type model for the magnetically active t_{2g} bands, by recasting the problem in the language of localized Wannier orbitals. Then, we map the obtained electron model onto the pseudospin model by applying the theory of SE interactions, which is based on the second-order perturbation theory with respect to the transfer integrals. We discuss the microscopic origin of anisotropic SE interactions, inherent to the compass Heisenberg model, and the appearance of the antisymmetric Dzyaloshinskii-Moriya term, associated with the additional rotation of the IrO_6 octahedra in Sr_2IrO_4. In order to solve the pseudospin Hamiltonian problem and evaluate the Néel temperature (T_N), we employ the nonlinear sigma model. We have found that, while for Sr_2IrO_4 our value of T_N agrees with the experimental data, for Ba_2IrO_4 it is overestimated by a factor of 2. We argue that this discrepancy is related to limitations of the SE model: while for more localized t_{2g} states in Sr_2IrO_4 it works reasonably well, the higher-order terms in the perturbation theory expansion play a more important role in the more "itinerant" Ba_2IrO_4, giving rise to the new type of isotropic and anisotropic exchange interactions, which are not captured by the SE model. This conclusion is supported by unrestricted Hartree-Fock calculations for the same electron model, where in the case of Ba_2IrO_4, already on the mean-field level, we were able to reproduce the experimentally observed magnetic ground state, while for Sr_2IrO_4 the main results are essentially the same as in the SE model.

DOI: 10.1103/PhysRevB.92.235109 PACS number(s): 75.85.+t, 75.25.−j, 71.15.Mb, 71.10.Fd

I. INTRODUCTION

5*d* transition-metal oxides have attracted a considerable attention as a new paradigm of relativistic magnetic materials, whose properties are largely influenced by the strong spin-orbit (SO) coupling, leading to the experimental realization and a number of theoretical proposals for such fascinating phenomena as SO interaction assisted Mott state in Sr_2IrO_4 [1–3], spin-liquid state in $Pr_2Ir_2O_7$ (Ref. [4]), and $Na_4Ir_3O_8$ (Refs. [5,6]), possible existence of topological semimetallic states in pyrochlore iridates [7], and unusual magnetic ordering in the honeycomb compounds Na_2IrO_3 and Li_2IrO_3 [8–11], which may be relevant to the Kitaev model of bond-dependent anisotropic magnetic coupling [12].

In this respect, a lot of attention is being focused on the properties of tetravalent iridium oxides (or iridates), originating from the $\frac{5}{6}$-filled Ir t_{2g} band, located near the Fermi level. The strong SO interaction splits the atomic t_{2g} states into the fully occupied fourfold degenerate $j = \frac{3}{2}$ states and twofold (Kramers) degenerate $j = \frac{1}{2}$ states, which accommodate one electron. In this sense, there is a clear analogy with the spin-$\frac{1}{2}$ systems and the problem of interatomic exchange interactions can be formulated in terms of some appropriately selected pseudospin states. In solids, each group of states form the bands, which can, however, overlap with each other. Moreover, since j is the band quantum number in solids, there is always a finite hybridization between these two groups of relativistic states. The $j = \frac{1}{2}$ electrons experience the onsite Coulomb repulsion and can polarize the occupied $j = \frac{3}{2}$ shell via the intraatomic exchange interactions. Moreover, the precise division of the t_{2g} states into the $j = \frac{3}{2}$ and $\frac{1}{2}$ ones depends on the crystal-field splitting, which is typically smaller than the SO coupling. These are the main ingredients, which predetermine the low-energy electronic properties of iridates.

The layered perovskites Sr_2IrO_4 and Ba_2IrO_4 are typically regarded as the key materials for revealing the basic microscopic mechanisms, which can operate in the iridates. They are also used as the benchmark materials for testing the new theoretical models. In this respect, the first and one of the most successful theoretical models for iridates was based on the Anderson theory of superexchange (SE) between t_{2g} electrons [13], which is valid in the limit of large onsite Coulomb repulsion and treats the transfer integrals between the Coulomb and SO interaction split t_{2g} levels in the second order of perturbation theory [6,14]. This model indeed reveals a rich and very interesting physics, including the bond dependence of the anisotropic exchange couplings and emergence of large antisymmetric Dzyaloshinskii-Moriya (DM) interactions when the inversion symmetry is broken by the antiphase rotations of the IrO_6 octahedra in Sr_2IrO_4.

*SOLOVYEV.Igor@nims.go.jp

At the same time, there was always a question about how far one can go in applying the SE model for the real iridates. For the layered systems, this point was raised in Ref. [15], where, using the dynamical mean-field theory (DMFT), the authors have argued that the behavior of both Sr_2IrO_4 and Ba_2IrO_4 retain many aspects of Slater insulators, whose insulating properties are closely related to the existence of the long-range antiferromagnetic (AFM) order. The problem reemerged again recently after the experimental discovery of the magnetic-ground-state structure of Ba_2IrO_4 [16], which cannot be described by the SE model, at least on the mean-field level [17]. It raises the question as to whether this magnetic ground state can be described by considering the quantum fluctuation effects, but within the SE model [17], or revising the SE model itself by including to it some higher-order terms in the perturbation theory expansion. The answer to this question is not obvious because, in the SE formulation, the effects of the SO coupling are included to the transfer integral. Therefore, the second-order perturbation theory with respect to the transfer integrals automatically means that it treats the SO coupling also only up to the second order. If the SO interaction is large (as in iridates), it can be a rather crude approximation because it does not take into account several important effects, such as the in-plane anisotropy in the uniaxial systems, which may be relevant to the experimentally observed behavior of Sr_2IrO_4 and Ba_2IrO_4. Another interesting point is the value of Néel temperature (T_N), which is remarkably close in both considered systems (about 240 K), and whether this fact can be rationalized on the basis of the SE theory or not.

The main purpose of this work is to critically reexamine abilities of the SE theory for the layered iridates. This is certainly not the first attempt to derive parameters of interatomic exchange interactions using the theory of SE interactions and the basic ideas of this method in the case of the strong SO coupling are well understood today, at least for the models [14,17–21]. Nevertheless, aside from the SO coupling, the behavior of interatomic exchange interactions strongly depends on the number of adjustable parameters, used in the model Hamiltonians, such as the onsite Coulomb and exchange interactions, tetragonal crystal-field splitting, and the matrices of transfer integrals. Therefore, we believe that, in the process of derivation of the pseudospin model, it is very important to reduce the number of possible ambiguities by sticking as much as possible to the first-principles electronic-structure calculations based on the density functional theory (DFT).

The rest of the paper is organized as follows. In Sec. II, we will briefly discuss the main differences of the crystal and electronic structures of Ba_2IrO_4 and Sr_2IrO_4. Then, in Sec. III we will explain our method of the construction of the effective low-energy electron model on the basis of DFT calculations with the SO coupling. This model will be further used in Sec. IV as the starting point for the derivation of the SE Hamiltonian in the basis of the pseudospin states. In Sec. V, we will discuss results of our calculations of the SE interactions and their implications to the magnetic properties of Ba_2IrO_4 and Sr_2IrO_4 using the nonlinear sigma model. Then, in Sec. VI, we will provide a detailed comparison with the results of unrestricted Hartree-Fock (HF) calculations, which do not rely on the perturbation theory, and argue that while for Sr_2IrO_4 the SE theory works reasonably well, for Ba_2IrO_4 it misses several important interactions, which are nonetheless captured by the HF calculations. Finally, in Sec. VII, we will give a brief summary of our work. Details of derivation of the nonlinear sigma model for the compass Heisenberg model will be given in the Appendix.

II. MAIN DETAILS OF CRYSTAL AND ELECTRONIC STRUCTURES

In this work we use the experimental structure parameters, reported in Refs. [22,23] (at 13 K) for Ba_2IrO_4 and Sr_2IrO_4, respectively. According to these data, Ba_2IrO_4 crystallizes in the undistorted tetragonal $I4/mmm$ structure with the Ir-O-Ir angles in the xy plane being equal to 180°. Sr_2IrO_4 exhibits the additional rotation of IrO_6 octahedra (the space group $I4_1/acd$), which leads to the deformation of the Ir-O-Ir bonds in the xy plane (see Fig. 1). Depending on the Ir site, this rotation can be either clockwise ($+\phi$) or counterclockwise ($-\phi$). The experimental value of the angle ϕ is 12° [23].

The corresponding electronic structure in the local-density approximation (LDA) with the SO coupling is displayed in Figs. 2 and 3 for Ba_2IrO_4 and Sr_2IrO_4, respectively. In this work, we will focus on the behavior of magnetically active Ir t_{2g} bands, located near the Fermi level and separated relatively well from the rest of the spectrum. There are two main differences between Ba_2IrO_4 and Sr_2IrO_4: (i) The Ir t_{2g} band is narrower in Sr_2IrO_4 (the bandwidth is about 3 and 3.5 eV in Sr_2IrO_4 and Ba_2IrO_4, respectively). This is generally consistent with the additional distortion in Sr_2IrO_4, which leads to the deformation of the Ir-O-Ir bonds. (ii) The Ba $5d$ band in Ba_2IrO_4, which strongly hybridizes and, therefore, has a large weight of the Ir $5d$ states, is much closer to the Fermi energy than the Sr $4d$ band in Sr_2IrO_4. This is mainly related to the larger Ba $5d$ bandwidth, due to the less distorted crystal structure as well as the relativistic effects [24].

In Ba_2IrO_4, the relativistic $j = \frac{3}{2}$ and $\frac{1}{2}$ subbands are separated by the direct gap, which allows us to construct both six- and two-orbital models (for the entire t_{2g} bands and $j = \frac{1}{2}$ subband, respectively). In Sr_2IrO_4, due to the

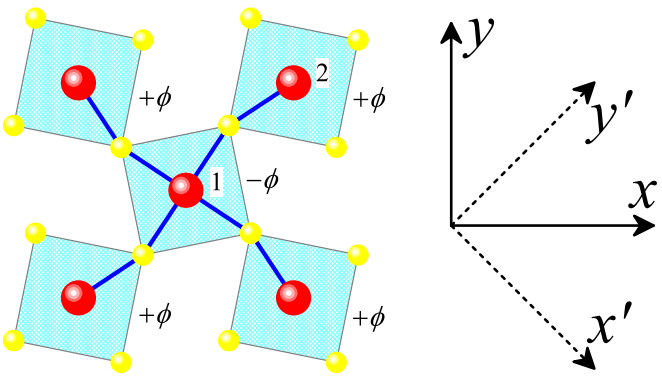

FIG. 1. (Color online) (Left) Rotations of IrO_6 octahedra in the xy plane of Sr_2IrO_4. The Ir atoms are indicated by the big (red) spheres and the oxygen atoms are indicated by the small (yellow) spheres. The sites around which the octahedra are rotated clockwise ($+\phi$) and counterclockwise ($-\phi$) are denoted as 2 and 1, respectively. (Right) The directions of axes in the $I4_1/acd$ (x,y) and $I4/mmm$ (x',y') coordinate frames.

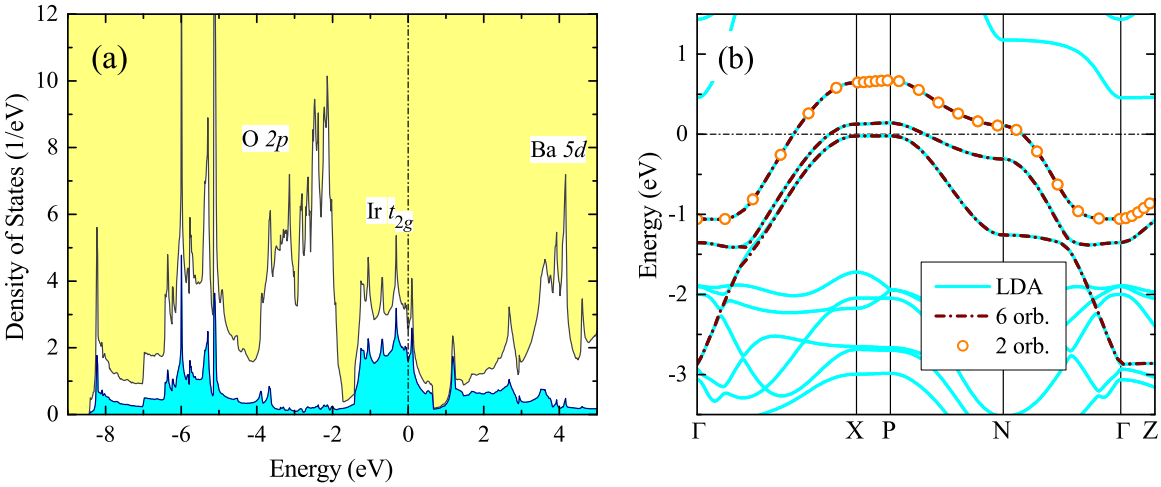

FIG. 2. (Color online) Electronic structure of Ba_2IrO_4 in LDA with the SO coupling. (a) Total and partial densities of states. The shaded area shows the contributions of the Ir 5*d* states. The positions of the main bands are indicated by symbols. (b) Band dispersion near the Fermi level, as obtained for the full LDA Hamiltonian in comparison with the six- and two-orbital models. The high-symmetry points of the Brillouin zone are denoted as $\Gamma = (0,0,0)$, $X = (\pi/a,\pi/a,0)$, $N = (\pi/a,0,\pi/c)$, $P = (\pi/a,\pi/a,\pi/c)$, and $Z = (0,0,2\pi/c)$. The Fermi level is at zero energy (shown by dotted-dashed line).

additional mixing between the $j = \frac{3}{2}$ and $\frac{1}{2}$ states, caused by the $I4_1/acd$ distortion, such separation does not take place. Therefore, for Sr_2IrO_4, we will focus only on the six-orbital model.

III. CONSTRUCTION OF EFFECTIVE LOW-ENERGY ELECTRON MODEL

In this section, we will discuss the construction of the low-energy electron model, starting from the LDA band structure with the SO interaction. For practical calculations, we use the linear muffin-tin orbital (LMTO) method in the nearly orthogonal representation [25]. The model itself has the following form:

$$\hat{\mathcal{H}}_{\rm el} = \sum_{ij}\sum_{\alpha\beta} t_{ij}^{\alpha\beta}\hat{c}_{i\alpha}^{\dagger}\hat{c}_{j\beta} + \frac{1}{2}\sum_{i}\sum_{\alpha\beta\gamma\delta} U_{\alpha\beta\gamma\delta}\hat{c}_{i\alpha}^{\dagger}\hat{c}_{i\gamma}^{\dagger}\hat{c}_{i\beta}\hat{c}_{i\delta}, \quad (1)$$

where $\hat{c}_{i\alpha}^{\dagger}$ and $\hat{c}_{i\alpha}$ are, respectively, the creation and annihilation operators of an electron on the Wannier orbitals $w_{i\alpha}$, centered at the Ir site i and specified by the index $\alpha = (m,s)$, which numbers Kramers doublets $m = 1$, 2, or 3 (an analog of orbital indices without SO coupling) and the states $s = 1$ or 2 within each such doublet (an analog of spin indices without SO coupling).

First, we construct the Wannier functions for the magnetically active bands, using the projector-operator technique [26–28]. We consider the six-orbital model for the both

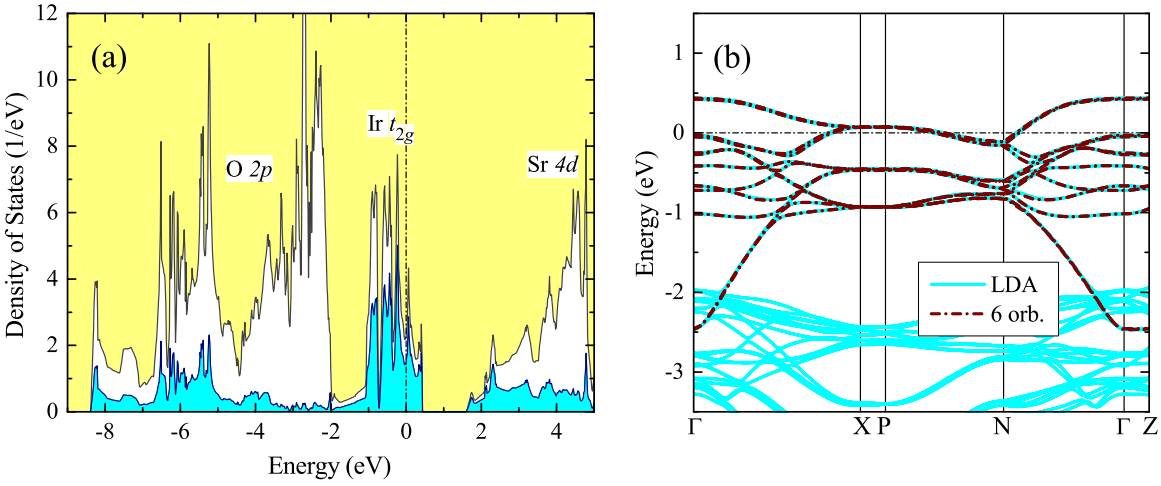

FIG. 3. (Color online) Electronic structure of Sr_2IrO_4 in LDA with the SO coupling. (a) Total and partial densities of states. The shaded area shows the contributions of the Ir 5*d* states. The positions of the main bands are indicated by symbols. (b) Band dispersion near the Fermi level, as obtained for the full LDA Hamiltonian in comparison the six-orbital models. The Fermi level is at zero energy (shown by dotted-dashed line).

Ba_2IrO_4 and Sr_2IrO_4. Moreover, for Ba_2IrO_4 it is also possible to construct the two-orbital model, by considering only two highest degenerate bands (see Fig. 2). The trial functions, which are used for the projection, were obtained from the digonalization of the site-diagonal density matrix, calculated for the magnetically active bands in the basis of the Ir $5d$ orbitals [26,28]. Namely, after the diagonalization of the density matrix, we pick up either six or two eigenstates (depending on the dimensionality of the model) with the largest eigenvalues and use them as the trial functions. Such construction guarantees that the Wannier functions are well localized in the real space: the main part of the density matrix with the largest eigenvalues is described by the "heads" of the Wannier functions, residing on the central site, and only a small remaining part of this matrix is described by the "tails" of the Wannier functions, coming from the neighboring Ir sites. Thus, the main weight of the Wannier function is concentrated in its "head" part, while the contribution of "tails" is relatively small. Such procedure was extensively used in nonrelativistic calculations without the SO coupling [26]. The new aspect of the relativistic formulation is that the eigenstates of the density matrix become Kramers degenerate. Therefore, the trial functions and the Wannier functions (w_1 and w_2) for each Kramers doublet can be chosen so to satisfy the conditions $|w_2\rangle = \hat{T}|w_1\rangle$ and $|w_1\rangle = -\hat{T}|w_2\rangle$, where $\hat{T} = i\hat{\sigma}_y\hat{K}$ is the time-reversal operation, written in terms of the spin Pauli matrix $\hat{\sigma}_y$ and the complex-conjugation operator $\hat{K}$.

Then, the one-electron part of the model Hamiltonian (1) is identified with the matrix elements of the LDA Hamiltonian in the Wannier basis: $t_{ij}^{\alpha\beta} = \langle w_{i\alpha}|\hat{\mathcal{H}}_{\rm LDA}|w_{j\beta}\rangle$. This procedure can be also reformulated as the downfolding of the LDA Hamiltonian [26,28]. Then, the site-diagonal matrix elements $t_{i=j}^{\alpha\beta}$ describe the splitting of the atomic levels by the crystal field and the SO interaction, while the off-diagonal elements $t_{i\neq j}^{\alpha\beta}$ stand for interatomic transfer integrals (or kinetic hoppings).

The matrix of screened onsite interactions $\hat{U} = [U_{\alpha\beta\gamma\delta}]$ has been calculated using a simplified version of the constrained random-phase approximation (RPA) [26]. The RPA is used in the GW method in order to evaluate the momentum and frequency dependence of the screened Coulomb interaction, which is then used in calculations of the self-energy [29]. The basic idea of the constrained RPA is to switch off some contributions to the RPA polarization function (and, therefore, to the screening of $\hat{U}$) related to the transition between the magnetically active bands (in our case, the Ir $5d$ bands) [30]. The RPA is inadequate for this channel of screening (especially when it is evaluated starting from the LDA band structure) and should be replaced by a more rigorous method in the process of solution of the low-energy model (1). The purpose of additional simplifications is to replace the time-consuming RPA for the screening, caused by the relaxation of the atomic wave function and other (non-$5d$) states, by much faster and more suitable for these purposes constrained LDA technique. After that, we consider (within RPA) the additional and most efficient channel of screening of the Coulomb interactions in the Ir $5d$ bands by (the same) Ir $5d$ states, which contribute to other parts of the electronic structure (mainly to the O $2p$ and either Ba $5d$ or Sr $4d$ bands in Figs. 2 and 3) due to the hybridization [26]. Such approximation incorporates the main channels of screening and, thus, reproduces reasonably well the values of static Coulomb interactions, obtained in full-scale constrained RPA calculations. The obtained matrix elements $U_{\alpha\beta\gamma\delta}$ have the following form:

$$U_{\alpha\beta\gamma\delta} = \int d\mathbf{r} \int d\mathbf{r}' w_\alpha^\dagger(\mathbf{r}) w_\beta(\mathbf{r}) v_{\rm scr}(\mathbf{r},\mathbf{r}') w_\gamma^\dagger(\mathbf{r}') w_\delta(\mathbf{r}'), \quad (2)$$

where the screened interaction $v_{\rm scr}(\mathbf{r},\mathbf{r}')$ in RPA is invariant under the time-reversal operation and does not depend on the spin variables.

IV. PSEUDOSPIN MODEL

In this section, we will consider the mapping of the electron model (1) onto the magnetic model, formulated in terms of *pseudospin* variables $\boldsymbol{\mathcal{S}}_i = (\mathcal{S}_i^x, \mathcal{S}_i^y, \mathcal{S}_i^z)$:

$$\hat{\mathcal{H}}_{\mathcal{S}} = \sum_{i>j} \boldsymbol{\mathcal{S}}_i \overleftrightarrow{\boldsymbol{J}}_{ij} \boldsymbol{\mathcal{S}}_j + \mu_{\rm B} \sum_i \boldsymbol{\mathcal{S}}_i \overleftrightarrow{\boldsymbol{g}}_i \boldsymbol{H}, \quad (3)$$

where $\overleftrightarrow{\boldsymbol{J}}_{ij}$ and $\overleftrightarrow{\boldsymbol{g}}_i$ are the 3×3 tensors, describing interactions in the system of pseudospins and with the external magnetic field $\boldsymbol{H}$, respectively. The pseudospin operators are represented by the Pauli matrices $\mathcal{S}_i^x = \frac{1}{2}\left(\begin{smallmatrix}0 & 1\\ 1 & 0\end{smallmatrix}\right)$, $\mathcal{S}_i^y = \frac{1}{2}\left(\begin{smallmatrix}0 & -i\\ i & 0\end{smallmatrix}\right)$, and $\mathcal{S}_i^z = \frac{1}{2}\left(\begin{smallmatrix}1 & 0\\ 0 & -1\end{smallmatrix}\right)$.

For each bond, $\overleftrightarrow{\boldsymbol{J}}_{ij}$ can be presented as the sum of its symmetric (S) and antisymmetric (A) components: $\overleftrightarrow{\boldsymbol{J}}_{ij} = \overleftrightarrow{\boldsymbol{J}}_{ij}^{(S)} + \overleftrightarrow{\boldsymbol{J}}_{ij}^{(A)}$, where $\overleftrightarrow{\boldsymbol{J}}_{ij}^{(S)} = \frac{1}{2}(\overleftrightarrow{\boldsymbol{J}}_{ij} + \overleftrightarrow{\boldsymbol{J}}_{ij}^T)$ and $\overleftrightarrow{\boldsymbol{J}}_{ij}^{(A)} = \frac{1}{2}(\overleftrightarrow{\boldsymbol{J}}_{ij} - \overleftrightarrow{\boldsymbol{J}}_{ij}^T)$. $\overleftrightarrow{\boldsymbol{J}}_{ij}^{(S)}$ incorporates all types of symmetric exchange interactions in the bond $i-j$, where the isotropic exchange interaction is defined as $J_{ij} = \frac{1}{3}{\rm Tr}\overleftrightarrow{\boldsymbol{J}}_{ij}^{(S)}$, while $\overleftrightarrow{\boldsymbol{J}}_{ij}^{(A)}$ describes anisotropic DM interactions. $\overleftrightarrow{\boldsymbol{J}}_{ij}^{(A)}$ has only three independent elements, which can be viewed as the components of some axial vectors (the so-called DM vector) $\boldsymbol{d}_{ij} = (d_{ij}^x, d_{ij}^y, d_{ij}^z)$:

$$\overleftrightarrow{\boldsymbol{J}}_{ij}^{(A)} = \begin{pmatrix} 0 & d_{ij}^z & -d_{ij}^y \\ -d_{ij}^z & 0 & d_{ij}^x \\ d_{ij}^y & -d_{ij}^x & 0 \end{pmatrix},$$

yielding the well-known identity $\boldsymbol{\mathcal{S}}_i \overleftrightarrow{\boldsymbol{J}}_{ij}^{(A)} \boldsymbol{\mathcal{S}}_j = \boldsymbol{d}_{ij}[\boldsymbol{\mathcal{S}}_i \times \boldsymbol{\mathcal{S}}_j]$.

A. Calculation of superexchange interactions

In this work, we follow the Anderson theory of superexchange (Ref. [13]) and apply it for the t_{2g} electrons in Ba_2IrO_4 and Sr_2IrO_4. In order to calculate the SE interactions, we adapt a standard procedure for the systems, where the degeneracy of the atomic states is lifted by the crystal field and the SO interaction. Namely, we assume that, in the atomic limit, the single hole resides on the highest Kramers doublet, obtained from the diagonalization of the site-diagonal part $\hat{t} = [t_{i=j}^{\alpha\beta}]$ of the one-electron Hamiltonian. The states $|\varphi_1\rangle$ and $|\varphi_2\rangle$ of this Kramers doublet are used for the construction of the eigenstates $|\pm x\rangle$, $|\pm y\rangle$, and $|\pm z\rangle$ of the pseudospin operators $\mathcal{S}^x$, $\mathcal{S}^y$, and $\mathcal{S}^z$, respectively. For convenience, we choose the phases of these states so that $|\varphi_2\rangle = \hat{T}|\varphi_1\rangle$ and $|\varphi_1\rangle = -\hat{T}|\varphi_2\rangle$.

Let us first explain the construction of $|\pm z\rangle$. For these purposes, one can choose any pair of states, which is obtained by the unitary transformation of $|\varphi_1\rangle$ and $|\varphi_2\rangle$. Moreover, since the states are degenerate, the transformation will not change the total energy, and the model (3) does not contain the single-ion anisotropy term. Then, we employ the fact that, despite some complications caused by the SO coupling, the magnetic moment will always have a finite spin component, and define the pseudospin states $|+z\rangle$ and $|-z\rangle$ as those corresponding to, respectively, the maximal and minimal projections of the spin onto the z axis. The problem is equivalent to the diagonalization of the 2×2 spin Pauli matrix $\hat{\sigma}_z$ in the basis of $|\varphi_1\rangle$ and $|\varphi_2\rangle$.

Then, one can readily define two other groups of states as $|\pm x\rangle = \frac{1}{\sqrt{2}}|+z\rangle \pm \frac{1}{\sqrt{2}}|-z\rangle$ and $|\pm y\rangle = \pm\frac{1-i}{2}|+z\rangle + \frac{1+i}{2}|-z\rangle$. In this construction, the phases of $|\pm z\rangle$ were chosen to satisfy the condition $\hat{T}|-z\rangle = |+z\rangle$ and $\hat{T}|+z\rangle = -|-z\rangle$. It allows us to define unambiguously all phases of $|\pm z\rangle$ but ζ, which transforms $|\pm z\rangle$ to $e^{\mp i\zeta}|\pm z\rangle$. The latter phase is defined so to satisfy the condition $\langle +x|\hat{\sigma}_y|+x\rangle = 0$.

In order to find $\overleftrightarrow{\boldsymbol{J}}_{ij}$, we evaluate the energy gain $\mathcal{T}_{ij}(a,b)$, caused by the virtual excitations of the hole from the ath orbital of the site i to the bth orbital of the site j and vice versa, in the second order of perturbation theory with respect to the transfer integrals $t^{\alpha\beta}_{i\neq j}$. The denominators in the SE theory are given by the energies of charge excitations $d^5_i d^5_j \rightarrow d^4_i d^6_j$, which are the energies of the two-hole states. In the process of virtual excitations, the Pauli exclusion principle was guaranteed by the projection operators, which permit the hoppings only between occupied and unoccupied orbitals. Moreover, for the excited two-hole states, the problem was solved in the true many-body fashion, by finding the eigenstates and the eigenenergies from the diagonalization of the Coulomb interaction matrix $\hat{U}$ in the basis of $\frac{6\times 5}{2} = 15$ Slater determinants, constructed from six atomic spin orbitals. This is the step beyond the mean-field approximation. It additionally stabilizes the AFM interactions [26]. Then, we consider all combinations of a and $b = \pm x, \pm y$, or $\pm z$, and map the obtained energy gains onto the pseudospin model (3) for $\boldsymbol{H} = 0$. This procedure was discussed in details in Ref. [31].

B. Calculation of g tensor

The g tensor describes the interaction of the pseudospin with the external magnetic field [see Eq. (3)]. In the SE approximation, it can be evaluated using Eq. (31.34) of Ref. [32], from which one can find all nine elements of the tensor $\overleftrightarrow{\boldsymbol{g}}$ at each site of the lattice: $\langle +z|(L_x+\sigma_x)|+z\rangle = g^{xz}$, $\langle +z|(L_y+\sigma_y)|+z\rangle = g^{yz}$, $\langle +z|(L_z+\sigma_z)|+z\rangle = g^{zz}$, $\langle -z|(L_x+\sigma_x)|+z\rangle = g^{xx} + ig^{xy}$, $\langle -z|(L_y+\sigma_y)|+z\rangle = g^{yx} + ig^{yy}$, and $\langle -z|(L_z+\sigma_z)|+z\rangle = g^{zx} + ig^{zy}$, where L_x, L_y, and L_z are the matrices of angular momentum operators in the Wannier basis. The basic idea here is in the spirit of the SE model: it is assumed that only the highest Kramers doublet is magnetically active and all the properties can be computed using the unperturbed wave functions of the highest doublet in the atomic limit. More rigorous quantum chemical methods can be found in Refs. [33,34]. It is easy to separate the spin $\overleftrightarrow{\boldsymbol{g}}_S$ and orbital $\overleftrightarrow{\boldsymbol{g}}_L$ contributions to the g tensor, by considering the matrix elements of only $\boldsymbol{\sigma}$ and $\boldsymbol{L}$, respectively.

V. RESULTS AND DISCUSSIONS

A. Two-orbital model for Ba_2IrO_4

The two-orbital model is the simplest model which can be considered. In Ba_2IrO_4, the "$j = \frac{1}{2}$" bands are separated from the rest of the spectrum (see Fig. 2) and the construction is rather straightforward. The form of transfer integrals in this case is very simple. Since $\hat{t}$ is Hermitian, each 2×2 matrix $\hat{t}_{ij} = [t^{\alpha\beta}_{ij}]$ satisfies the property $\hat{t}_{ji} = \hat{t}^{\dagger}_{ij}$. Then, since all Ir sites are located in the inversion centers and connected by the translations, it holds $\hat{t}_{ji} = \hat{t}_{ij}$ and, therefore, $\hat{t}_{ij} = \hat{t}^{\dagger}_{ij}$. Finally, since $\hat{\mathcal{H}}_{\rm LDA}$ is invariant under the time-reversal operation, we will have two more identities: $(t^{11}_{ij})^* = t^{22}_{ij}$ and $(t^{12}_{ij})^* = -t^{21}_{ij}$, which can be obtained from $(t^{\alpha\beta}_{ij})^* = \langle \hat{T} w_{i\alpha}|\hat{T}\hat{\mathcal{H}}_{\rm LDA}|w_{j\beta}\rangle$. Thus, in the two-orbital model, each $\hat{t}_{ij}$ is proportional to the unity matrix $\hat{t}_{ij} = t_{ij}\hat{1}$ in the subspace spanned by the indices $\alpha(\beta) = 1$ and 2, where t_{ij} is a real constant.

The behavior of t_{ij} is explained in Fig. 4. As expected, the strongest hopping occurs between nearest neighbors in the xy plane. There are also finite hoppings between next-nearest neighbors in and between the planes.

Since $\hat{t}_{ij} = t_{ij}\hat{1}$, all SE interactions in the two-orbital model are isotropic. They can be easily evaluated using the formula $J_{ij} = 4t^2_{ij}/\mathcal{U}$ [13], where $\mathcal{U} = 1.52$ eV is the effective onsite Coulomb repulsion, obtained in the constrained RPA for the two-orbital model. Then, using the values of transfer integrals, displayed in Fig. 4, we will obtain $J_{ij} =$ 122.8, 2.5, and 0.8 meV for the nearest-neighbor (NN), next-NN, and interplane interactions, respectively. Since $J_{ij} > 0$, all interactions are antiferromagnetic.

B. Six-orbital model for Ba_2IrO_4

The atomic t_{2g} states are split into three doubly degenerate groups of levels, which in Ba_2IrO_4 are located at -209, -149, and 358 meV, relative to their center of gravity. Two lowest doublets correspond to $j = \frac{3}{2}$ and the highest one – to $j = \frac{1}{2}$. Thus, the splitting between the $j = \frac{1}{2}$ and $\frac{3}{2}$ states, which measures the strength of the SO coupling is very large. This justifies the use of the regular (nondegenerate) theory for the SE interactions.

For the tetragonal compounds, the eigenstates $|+z\rangle$ (and $|-z\rangle = -\hat{T}|+z\rangle$), corresponding to the highest Kramers doublet, can be decomposed in the basis of xy, yz, zx, and x^2-y^2 Wannier orbitals with both projections of spins:

$$\begin{aligned}|+z\rangle = {} & c^{\uparrow}_{xy}|w_{xy,\uparrow}\rangle + c^{\uparrow}_{yz}|w_{yz,\uparrow}\rangle + c^{\uparrow}_{zx}|w_{zx,\uparrow}\rangle \\ & + c^{\uparrow}_{x^2-y^2}|w_{x^2-y^2,\uparrow}\rangle + c^{\downarrow}_{xy}|w_{xy,\downarrow}\rangle + c^{\downarrow}_{yz}|w_{yz,\downarrow}\rangle \\ & + c^{\downarrow}_{zx}|w_{zx,\downarrow}\rangle + c^{\downarrow}_{x^2-y^2}|w_{x^2-y^2,\downarrow}\rangle. \qquad (4)\end{aligned}$$

Due to the symmetry constraint, the $3z^2 - r^2$ orbitals do not contribute to $|+z\rangle$. The coefficients in this expansion

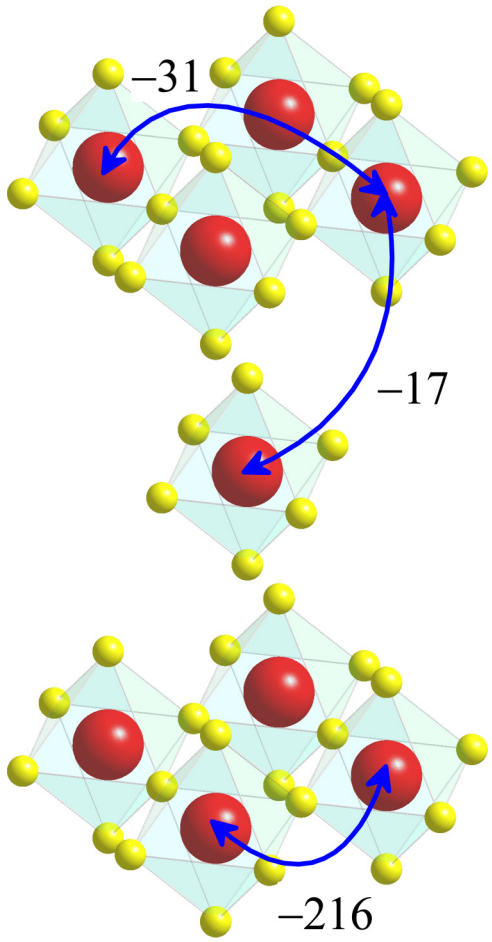

FIG. 4. (Color online) Crystal structure and transfer integrals (in meV) associated with different Ir-Ir bonds in the two-orbital model for Ba_2IrO_4. The Ir atoms are indicated by the big (red) spheres and the oxygen atoms are indicated by the small (yellow) spheres.

depend on the relative strength of the crystal-field splitting and the SO interaction. They cannot be determined solely from the symmetry considerations. For Ba_2IrO_4, we obtain the following (nonvanishing) coefficients in the $I4/mmm$ coordinate frame: $c^{\downarrow}_{x'y'} = -i0.522$, $c^{\uparrow}_{z'x'} = -ic^{\uparrow}_{y'z'} = 0.603$, and $c^{\downarrow}_{x'^2-y'^2} = -0.004$, which correspond to $c^{\downarrow}_{xy} = 0.004$, $c^{\uparrow}_{zx} = -ic^{\uparrow}_{yz} = 0.426 + i0.426$, and $c^{\downarrow}_{x^2-y^2} = -i0.522$ in the $I4_1/acd$ frame.

The strongest transfer integrals, operating between the nearest neighbors in the xy plane, have the following form (in meV):

$$\hat{t}_{\langle ij\rangle||x',y'} = \begin{pmatrix} -283 & 0 & 0 & \pm 60 & 0 & -i76 \\ 0 & -283 & \mp 60 & 0 & -i76 & 0 \\ 0 & \mp 60 & -165 & 0 & \pm i92 & 0 \\ \pm 60 & 0 & 0 & -165 & 0 & \mp i92 \\ 0 & i76 & \mp i92 & 0 & -226 & 0 \\ i76 & 0 & 0 & \pm i92 & 0 & -226 \end{pmatrix}, \quad (5)$$

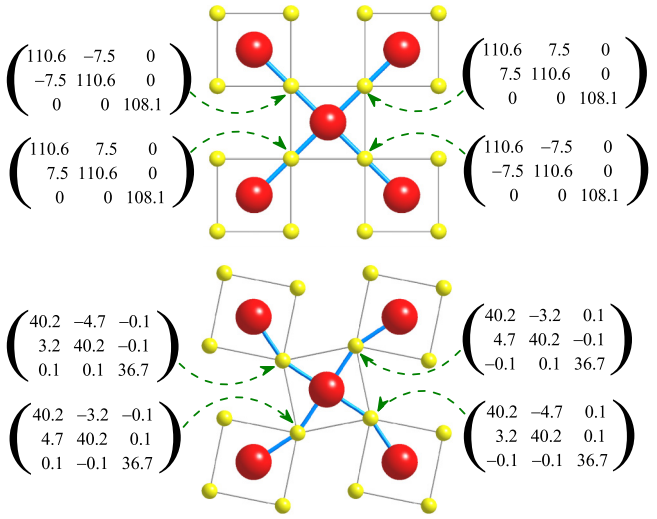

FIG. 5. (Color online) Tensors of superexchange interactions $\overleftrightarrow{J}_{ij}$ (in meV), as obtained in the six-orbital model for different Ir-Ir bonds in the xy plane of Ba_2IrO_4 (top) and Sr_2IrO_4 (bottom). The Ir atoms are indicated by the big (red) spheres and the oxygen atoms are indicated by the small (yellow) spheres. For the sake of convenience, the parameters for both structures are shown in the $I4_1/acd$ coordinate frame.

where the upper (lower) sign stands for the bonds parallel to the x' (y') axis in the $I4/mmm$ coordinate frame (see Fig. 5). Here, the matrix is given in the local representation, which diagonalizes the site-diagonal part of the one-electron Hamiltonian $[t^{\alpha\beta}_{i=j}]$, as described in Sec. IV A. Moreover, we adapt the following order of the Wannier orbitals: $(m,s) = (1,1)$, $(1,2)$, $(2,1)$, $(2,2)$, $(3,1)$, and $(3,2)$, where m numbers the Kramers doublet in the increasing order of their energies and s number the states within each doublet. Similar to the two-orbital model, the matrix elements of $\hat{t}_{ij}$ with same m do not depend on the s indices and each such subblock is proportional to the 2×2 unity matrix. However, there is a finite coupling between states with different m's. This coupling gives rises to the anisotropy of $\overleftrightarrow{J}_{ij}$. Moreover, since the signs of some of these matrix elements alternate between the bonds parallel to the x' and y' axes, the anisotropic part of $\overleftrightarrow{J}_{ij}$ will also alternate in the $x'y'$ plane. Another important factor, which is responsible for anisotropic properties of $\overleftrightarrow{J}_{ij}$, is the intraatomic exchange interaction $\mathcal{J}$ [14]. It will be discussed below. Other parameters of the model Hamiltonian can be found elsewhere [35].

The form of the screened onsite interactions $U_{\alpha\beta\gamma\delta}$ in the basis of relativistic Wannier orbitals is rather complex. Nevertheless, the main details of these interactions can be understood by considering the energies of two-hole excitations, which contribute to the SE processes (see Fig. 6). These energies were calculated using the matrices of screened Coulomb interactions $[U_{\alpha\beta\gamma\delta}]$, for which $v_{\rm scr}(\mathbf{r},\mathbf{r}')$ was obtained for two types of the electronic structures: with and without the SO coupling [see Eq. (2)]. In order to evaluate the averaged values of screened Coulomb and exchange interactions, we consider here only the effect of the matrix $[U_{\alpha\beta\gamma\delta}]$ and neglect the splitting of

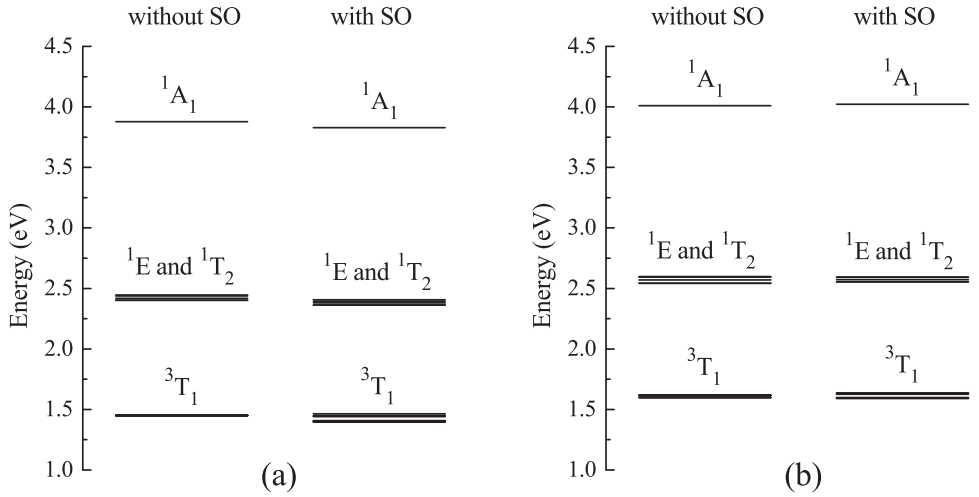

FIG. 6. The energies of two-hole states for Ba_2IrO_4 (a) and Sr_2IrO_4 (b), obtained using parameters of screened Coulomb interactions $U_{\alpha\beta\gamma\delta}$ for the six-orbital model with and without the spin-orbit (SO) coupling.

the two-hole states caused by the direct contributions of the SO interaction and the tetragonal distortion. The latter two contributions have been discussed in Ref. [19]. In the case of perfect cubic environment and without the SO coupling, the two-hole states are split into three groups: $^3T_1$, degenerate $^1T_2$ and ^1E, and $^1A_1$ with the energies $(\mathcal{U}-3\mathcal{J})$, $(\mathcal{U}-\mathcal{J})$, and $(\mathcal{U}+2\mathcal{J})$, respectively [36], in terms of the Kanamori parameters of the intraorbital Coulomb interaction $\mathcal{U}$ and the exchange interaction $\mathcal{J}$ [37]. The tetragonal environment of the $^{4+}$Ir ions, realized in Ba_2IrO_4, slightly lifts the degeneracy of the $^1T_2$ and ^1E states. The SO interaction further lifts the degeneracy of the $^3T_1$ states. However, in all other respects the positions of the main energy levels are very similar with and without the SO interactions. The (averaged) parameters $\mathcal{U}$ and $\mathcal{J}$ can be evaluated from the centers of gravity of the three groups of levels. This yields $\mathcal{U}=2.86$ (2.91) eV and $\mathcal{J}=0.48$ (0.49) eV with (without) SO interaction. Thus, $\mathcal{U}$ is generally larger in the six-orbital model, in comparison with the two-orbital one, due to the additionally screened by the $j=\frac{3}{2}$ electrons, which is included in the two-orbital model but not in the six-orbital one.

The parameters of the NN SE interactions in the xy plane are explained in Fig. 5. Since $J_{ij}^{xx}=J_{ij}^{yy}>J_{ij}^{zz}$, these parameters favor the in-plane configuration of the pseudospins, in agreement with the experiment [16]. Moreover, the phase of the off-diagonal element J_{ij}^{xy} (in the $I4_1/acd$ coordinate frame) is bond dependent, giving rise to the quantum compass interaction term. In the more conventional $I4/mmm$ coordinate frame, the tensor $\overleftrightarrow{\boldsymbol{J}}_{ij}$ is diagonal. The corresponding parameters are given by $J_{ij}^{x'x'}=J_{ij}^{xx}\pm|J_{ij}^{xy}|$ and $J_{ij}^{y'y'}=J_{ij}^{xx}\mp|J_{ij}^{xy}|$, where the upper (lower) sign stands for the bonds parallel to the x' (y') axis. The isotropic part $J_{ij}=\frac{1}{3}(J_{ij}^{xx}+J_{ij}^{yy}+J_{ij}^{zz})\equiv J_{12}=109.8$ meV is close to the value $J_{12}=123$ meV, obtained in the two-orbital model. This is mainly because of the combination of two effects: On the one hand, $\mathcal{U}$ is larger in the six-orbital model, which should lead to the smaller J_{12}. This decrease of J_{12} is partly compensated by somewhat stronger transfer integrals, operating between orbitals belonging to the highest Kramers doublet (-226 meV instead of -216 meV in the two-orbital model).

Our value of averaged in-plane interaction $J_{\rm av}=\frac{1}{2}(J_{12}^{xx}+J_{12}^{yy})=110.6$ meV is substantially larger than 65 meV, obtained in Ref. [17] on the basis of quantum chemical calculations. There may be several reasons for it. On the one hand, the exchange parameters reported in Ref. [17] were derived from the total energy difference of the states in a cluster. This procedure may include some other effects, which are formally beyond the SE processes and cannot be described by the bilinear type of interactions in the pseudospin Hamiltonian. This finding is consistent with the results of our total energy HF calculations, which will be discussed in Sec. VI: the effective interaction, derived from the total energies, is indeed smaller than in the SE model. However, we believe that this difference is actually the measure of biquadratic (or ring-type) interactions, existing in the system, which cannot be described properly by the SE Hamiltonian (3). On the other hand, the quantum chemical calculations explicitly take into account all contributions of the oxygen states, which can further decrease the AFM coupling [38].

As was already mentioned before, there are two important factors, which lead to the anisotropy of $\overleftrightarrow{\boldsymbol{J}}_{ij}$: (i) finite transfer integrals, connecting the states with $j=\frac{3}{2}$ and $\frac{1}{2}$ [see Eq. (5)] and (ii) finite intraatomic exchange coupling $\mathcal{J}$ [14], which lifts the main degeneracy of the virtual two-hole states (see Fig. 6). For instance, using the same transfer integrals, but simplified matrix of the screened onsite Coulomb interactions, which was reconstructed from averaged $\mathcal{U}=2.86$ eV and $\mathcal{J}=0$, we have obtained totally isotropic tensor $\overleftrightarrow{\boldsymbol{J}}_{ij}\equiv J_{ij}\overleftrightarrow{\mathbf{1}}$, where $\overleftrightarrow{\mathbf{1}}$ is the 3×3 unity tensor and $J_{ij}=71$ meV.

C. Six-orbital model for Sr_2IrO_4

In the case of Sr_2IrO_4, the splitting of the t_{2g} levels is -431, -4, and 435 meV. The symmetry properties of the $|+z\rangle$ orbital are given by the same Eq. (4) with the following (nonvanishing) coefficients: $c_{xy}^{\downarrow}=-0.015\mp i0.087$, $c_{zx}^{\uparrow}=-ic_{yz}^{\uparrow}=$

$\pm 0.184 + i0.643$, and $c^{\downarrow}_{x^2-y^2} = \pm 0.004 - i0.311$, where the upper (lower) sign is referred to the site 1 (2), experiencing the counterclockwise (clockwise) rotation of the IrO_6 octahedra (see Fig. 1).

In the local representation, which diagonalizes the site-diagonal part $[t^{\alpha\beta}_{i=j}]$ of the one-electron Hamiltonian, the matrix of transfer integrals between NN sites in the xy planes is given by (in meV)

$$\hat{t}_{\langle ij\rangle||x',y'} = \begin{pmatrix} 218+i60 & 0 & 0 & \mp 24 \mp i11 & 0 & 4-i38 \\ 0 & 218-i60 & \pm 24 \mp i11 & 0 & -4-i38 & 0 \\ 0 & \mp 24 \pm i11 & -94-i69 & 0 & \pm 29 \mp i68 & 0 \\ \pm 24 \pm i11 & 0 & 0 & -94+i69 & 0 & \pm 29 \pm i68 \\ 0 & -4-i38 & \mp 29 \pm i68 & 0 & -144-i7 & 0 \\ 4-i38 & 0 & 0 & \mp 29 \mp i68 & 0 & -144+i7 \end{pmatrix},$$

where the upper (lower) sign stands for the bond parallel to the x' (y') axis (see Fig. 1 for the notations). This matrix has both Hermitian $\hat{t}^{\rm h}_{ij} = \frac{1}{2}(\hat{t}_{ij} + \hat{t}_{ji})$ and anti-Hermitian $\hat{t}^{\rm ah}_{ij} = \frac{1}{2}(\hat{t}_{ij} - \hat{t}_{ji})$ parts. The Hermitian part has the same form as for Ba_2IrO_4 and gives rise to the symmetric anisotropic interactions $\overleftrightarrow{J}^{(S)}_{ij}$. The alternation of signs of some of these matrix elements will also lead to the alternation of anisotropic interactions in the xy plane. The anti-Hermitian part is the new aspect, which is related to the fact that the neighboring Ir sites in the $I4_1/acd$ structure are no longer connected by the inversion operation. This part is responsible for the DM interactions. The transfer integrals, involving the highest Kramers doublet, are generally smaller in Sr_2IrO_4 in comparison with Ba_2IrO_4, mainly due to the additional deformation of the Ir-O-Ir bonds and the more remote location of the Sr $4d$ states in the high-energy part of the spectrum (see Fig. 3). Therefore, the SE interactions are also expected to be smaller in Sr_2IrO_4.

Due to the additional symmetry lowering, the matrix of the screened Coulomb interactions $[U_{\alpha\beta\gamma\delta}]$ is even more complex than in Ba_2IrO_4. Nevertheless, the energies of the two-hole states, obtained from $[U_{\alpha\beta\gamma\delta}]$, have the same "three-level" structure as in Ba_2IrO_4, which is only slightly deformed by the lattice distortion and the SO interaction (see Fig. 6). The averaged parameters $\mathcal{U}$ and $\mathcal{J}$ can be again evaluated from the splitting between these three groups of levels as $\mathcal{U} = 3.05$ eV and $\mathcal{J} = 0.48$ eV (both with and without the SO interaction). The value of $\mathcal{J}$ is comparable with the one in Ba_2IrO_4. However, the Coulomb repulsion $\mathcal{U}$ is slightly larger in Sr_2IrO_4. This behavior is consistent with the change of the electronic structure (see Figs. 2 and 3): since the unoccupied Ba $5d$ states are closer to the Fermi level and strongly hybridize with the Ir $5d$ states, the Coulomb $\mathcal{U}$ is expected to be more screened in Ba_2IrO_4 than in Sr_2IrO_4 [26]. Moreover, it is reasonable to expect that the additional $I4_1/acd$ distortion in the case of Sr_2IrO_4 will make the t_{2g} states more localized and, thus, the screening of $\mathcal{U}$ less efficient. This will further reduce the values of the SE interactions in Sr_2IrO_4.

Considering only the values of interorbital Coulomb interactions $\mathcal{U}' = \mathcal{U} - 2\mathcal{J} = 1.90$ eV and 2.09 eV for Ba_2IrO_4 and Sr_2IrO_4, respectively, we note a reasonable agreement with the results full-scale constrained RPA calculations reported in Ref. [15] ($\mathcal{U}'$ is about 1.47 and 1.77 eV for Ba_2IrO_4 and Sr_2IrO_4, respectively). Moreover, the authors of Ref. [15] used a simplified $I4/mmm$ structure and theoretical lattice parameters both for Ba_2IrO_4 and Sr_2IrO_4, which may lead to the additional screening of $\mathcal{U}'$. A more serious discrepancy is found for $\mathcal{J}$: our value of $\mathcal{J}$ is close to the atomic one, which seems to be reasonable, because $\mathcal{J}$ is only weakly screened in the RPA [39]. However, the values of $\mathcal{J}$ reported in Ref. [15] are about three times smaller, leading to the violation of the Kanamori rule $\mathcal{U}' = \mathcal{U} - 2\mathcal{J}$, presumably due to the contribution of the oxygen states to the Wannier functions [40]. This itself is an interesting point because, according to Ref. [14], smaller value of $\mathcal{J}$ within the spherical model, which respects the Kanamori rule, should reduce the anisotropy of the exchange interactions. Therefore, it is interesting to which extent this anisotropy of the exchange interactions will be compensated by the anisotropy of the Coulomb interactions, which emerges in the full-scale constrained RPA calculations and manifested in the violation of the Kanamori rule. In any case, according to the analysis of the effective electron model based on the dynamical mean-field theory [15], our values of the parameters $\mathcal{U}$ and $\mathcal{U}'$ should correspond to the insulating behavior for Ba_2IrO_4 and Sr_2IrO_4, thus justifying the use of the $\hat{t}/\mathcal{U}$ expansion for the analysis of interatomic exchange interactions.

The $I4_1/acd$ structure of Sr_2IrO_4 contains two IrO_2 planes. The behavior of NN SE interactions in one of the planes is explained in Fig. 5. The parameters in another plane can be obtained by the 90° rotation about the z axis. As was expected, the isotropic part of the exchange interactions $J_{12} = \frac{1}{3}(J^{xx}_{12} + J^{yy}_{12} + J^{zz}_{12}) = 39.0$ meV is considerably smaller than in Ba_2IrO_4.

It should be noted that the magnon dispersion in Sr_2IrO_4, measured by the resonant inelastic x-ray scattering, can be fitted in terms of first-, second-, and third-neighbor interactions in the xy plane, which are 60, -20, and 15 meV, respectively [41]. Recently, this finding was also confirmed by the x-ray resonant magnetic scattering measurements [42]. The first-neighbor interaction is larger than 39 meV, obtained in this work in the framework of the SE model. However, an even more surprising fact is that the fit of the experimental dispersion requires comparable exchange interactions, spreading up to at least third-nearest neighbors in the xy plane. It is definitely inconsistent with the results of the SE model, where the exchange interactions are short ranged and limited by the nearest (first) neighbors. Moreover, as we will see in Sec. VI, the biquadratic exchange interactions, which arise beyond the SE approximation for the same effective electron model and

which are expected to be small in Sr_2IrO_4, seem to be not sufficient to explain such discrepancies. Thus, it is still an open question as to which ingredients should be additionally included to the electron model in order to describe properly the experimental magnon dispersion. It is definitely a challenging issue for the future studies.

Since $J_{12}^{xx} = J_{12}^{yy} > J_{12}^{zz}$, the pseudospins will favor the in-plane configuration, similar to Ba_2IrO_4 and in agreement with the experimental situation [3,43]. In Sr_2IrO_4, the parameter of the easy-plane anisotropy for the NN interactions $\Delta_\lambda = 1 - J_{12}^{zz}/J_{12}^{xx}$ has been recently estimated in the x-ray resonant magnetic scattering experiments as 0.08 [42], which is close to our theoretical value of 0.087. The symmetric anisotropic part of $\overleftrightarrow{J}_{12}$ is $|J_{12}^{(S)xy}| \equiv \Delta J_{12} = 0.73$ meV, which is about one order of magnitude smaller than in Ba_2IrO_4. This interaction is also bond dependent.

The antisymmetric part of $\overleftrightarrow{J}_{12}$ can be represented in terms of the DM vector (in meV): $\boldsymbol{d}_{12} = (-0.1, -0.1, -3.97)$ (see Fig. 1 for the notations of atomic sites). The phases of d^x and d^y alternate in the four NN bonds around the site 1. Since all NN atoms, surrounding the site 1, have the same direction of the pseudospin, the total contribution of d^x and d^y to the canting of these pseudospins will vanish. On the other hand, the phases of d^z are the same for all NN bonds. Thus, d^z will be responsible for the ferromagnetic (FM) canting, which can be estimated as $|d_{12}^z/(2J_{12}^{xx})| \sim 2.8^\circ$. This value is smaller than the experimental estimate of 8° [1]. Therefore, the weak FM moment is also expected to be smaller. Indeed, according to the unrestricted HF calculations, which will be discussed in Sec. VI, the weak FM moment is about 0.03 μ_B/Ir, while the experimental estimates range from 0.06 μ_B/Ir (Ref. [44]) until 0.10 μ_B/Ir (Ref. [3]). Nevertheless, the negative sign of d^z for the bond 1-2 is consistent with the counterclockwise rotation of the IrO_6 octahedra [14]. This picture can be also verified experimentally [45].

The weak ferromagnetism in Sr_2IrO_4 is the very important issue, which we would like to discuss more in details. According to the first-principles GGA + U calculations (where GGA stands for the gradient corrected approximation), the canted AFM ground state is highly sensitive to small structural deformations and the use of the experimental crystal structure in the theoretical calculations yields somewhat smaller canting [46]. This is partly consistent with our finding because all our calculations have been also performed for the experimental crystal structure. In order to further clarify this issue, we have also performed the LDA + U calculations using ELK full-potential package (and the values $U = 3$ eV and $J_H = 0.48$ eV for the onsite Coulomb and exchange interaction, respectively) [47]. We were able to reproduce the AFM ground state, where the magnetic moments are mainly parallel to the x axis and ferromagnetically canted along the y axis. The corresponding values of the spin and orbital magnetic moments at the Ir sites are 0.095 μ_B and 0.305 μ_B. By considering only Ir sites, the canting of spin, orbital, and total moments can be estimated as 13.9°, 12.3°, and 12.6°, respectively, and the weak net magnetic moment is 0.087 μ_B. All these values are consistent with those reported in Ref. [46]. However, this is only part of the story because there is also a contribution to the net magnetic moment coming from the oxygen sites. In the ELK calculations, the spin and orbital magnetic moments at the oxygen sites are about 0.006 μ_B and 0.005 μ_B, respectively. These moments are small. However, they are canted along the y axis by 51.3° and 53.1°, respectively. Due to such large canting, the oxygen sites produce an appreciable contribution to the net magnetic moment, which can be estimated as 0.018 μ_B (taking into account the contributions of two oxygen sites in the xy plane). Thus, our conclusion is that there is an important piece of physics, related to the magnetic polarization of the oxygen states, which is not properly captured by the model Hamiltonian (3). Therefore, we believe that the small value of d_{12}^z and, therefore, the spin canting, obtained in our work, is partly due to internal limitations of the SE model, which does not explicitly treat the contributions of the oxygen states. This conclusion is partly supported by the results of Ref. [46]. The authors of this work attempted to derive parameters of the magnetic model using the constrained density functional theory, where they fixed the directions of the magnetic moments *only at the Ir sites* (and fully relax the contributions of the oxygen sites), calculated the total energy, and then mapped them onto the model Hamiltonian of the form (3). They obtained the following values of the isotropic exchange and DM interactions in the xy plane (in our notations): $J_{12} = 22.2$ meV and $d^z = -17.4$ meV. They correspond to the FM canting of 21.4°, which is substantially larger than the experimental value and also the value obtained in Ref. [46] in the direct (unconstrained) optimization of the magnetic structure. Although the procedure, which was employed in Ref. [46] for the construction of the magnetic Hamiltonian, is very different from the one we use in this work, such inconsistency also means that some important information is missing in the process of the construction of the model Hamiltonian and this information is probably related to the polarization of the oxygen sites.

For Sr_2IrO_4, the parameters of interatomic exchange interactions have been also computed in Ref. [34], by mapping the total energies, obtained in the quantum chemical calculations, onto the pseudospin model (3). The obtained values $J_{12} = 47.8$ meV and $\Delta J_{12} = 0.63$ meV are in reasonable agreement with our finding. However, the DM interaction $d_{12}^z = -11.9$ meV is about three times larger than ours. This difference may be also related to the effect of the oxygen states, which are explicitly taken into account in the quantum chemical calculations.

D. Roles of the tetragonal splitting

Without SO interaction, the tetragonal distortion splits the t_{2g} manifold into the nondegenerate $x'y'$ and doubly degenerate $(y'z', z'x')$ states. The parameter of the tetragonal splitting $\Delta_{t_{2g}}$ is defined as the energy difference between these groups of levels. In our notations, $\Delta_{t_{2g}} < 0$ means that the $x'y'$ orbital is located higher in energy (and vice versa). $\Delta_{t_{2g}}$ is the very important parameter, which controls the properties of layered perovskites. In iridates, the importance of such control was emphasized recently in Ref. [34]. Particularly, on the basis of quantum chemical calculations, it was predicted that the t_{2g} levels have different order in Ba_2IrO_4 and Sr_2IrO_4, that is reflected in the anisotropy of the g tensor, which also behaves differently in Ba_2IrO_4 ($g^{xx} = g^{yy} > g^{zz}$) and Sr_2IrO_4

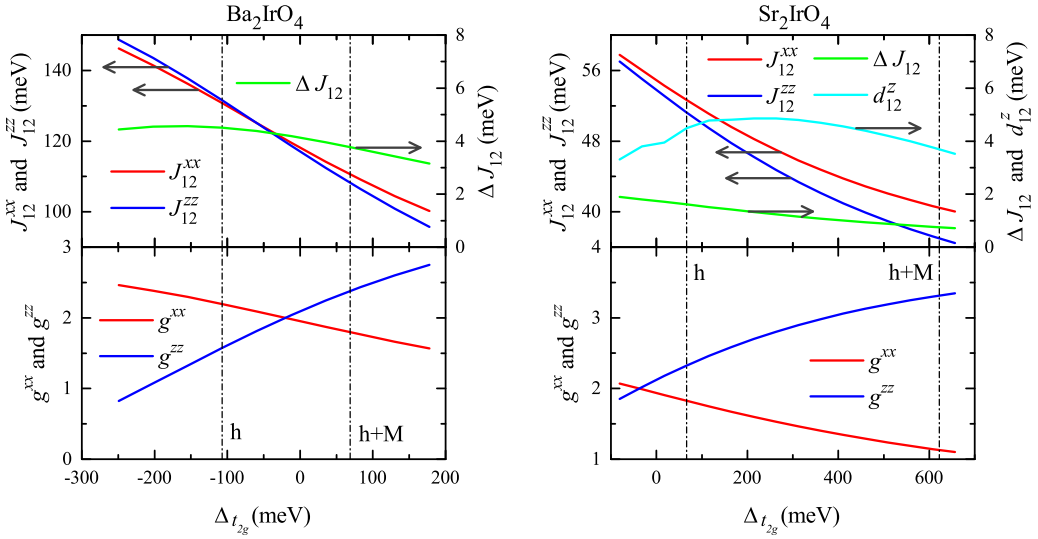

FIG. 7. (Color online) Parameters of pseudospin Hamiltonian (3) versus the tetragonal splitting between t_{2g} levels for Ba_2IrO_4 (left) and Sr_2IrO_4 (right). Two vertical lines show the calculated splitting, which is caused by the hybridization effects alone (h), and the combined effect of the hybridization and the nonsphericity of the Madelung potential (h+M).

($g^{xx} = g^{yy} < g^{zz}$). For Sr_2IrO_4, this finding was confirmed by the electron spin resonance measurements. The off-diagonal element g^{xy}, associated with the rotation of the IrO_6 octahedra in Sr_2IrO_4, is small and we do not discuss it here.

Taking into account the importance of this problem, we discuss it in this section more in details, treating $\Delta_{t_{2g}}$ as a parameter. The results of such calculations for the NN exchange interactions and the g tensor are presented in Fig. 7.

The IrO_6 octahedra are elongated along the z axis both in Ba_2IrO_4 and Sr_2IrO_4 (the corresponding elongation is 7% and 4%, respectively) [22,23]. Thus, the distortions of the IrO_6 octahedra alone will hardy explain the difference between Ba_2IrO_4 and Sr_2IrO_4, which should be associated with more subtle aspects of the crystal and electronic structures of these compounds.

There are several contributions to the tetragonal level splitting [26]. The first one is related to the hybridization (or covalent mixing) of atomic orbitals, which affects the shape of the Wannier functions of the $x'y'$ and $(y'z',z'x')$ symmetry and, thus, results in the crystal-field splitting between these two groups of states. It can be easily evaluated in the framework of the LMTO method [25], which relies on the spherical symmetrization of the LDA potential within atomic spheres and, therefore, does not produce any other contributions to the crystal field, except the ones related to the hybridization. The hybridization effects alone do produce the different order of the t_{2g} levels in the case of Ba_2IrO_4 and Sr_2IrO_4: $\Delta^{\rm h}_{t_{2g}} = -107$ and 67 meV, respectively. These values are roughly consistent with those obtained by Bogdanov *et al.* (note that our $\Delta_{t_{2g}}$ is defined with the opposite sign) [34]. The corresponding matrix elements of the g tensor, $g^{xx} = 2.20$ (1.83) and $g^{zz} = 1.57$ (2.33) for Ba_2IrO_4 (Sr_2IrO_4), are also in reasonable agreement with those obtained by Bogdanov *et al.* [34], thus confirming the change of the anisotropy of the g tensor from $g^{xx} = g^{yy} > g^{zz}$ in Ba_2IrO_4 to $g^{xx} = g^{yy} < g^{zz}$ in Sr_2IrO_4. Nevertheless, the splitting of the t_{2g} levels also affects the behavior of interatomic exchange interactions and *their anisotropy*. This point appears to be especially important for Ba_2IrO_4 because for $\Delta^{\rm h}_{t_{2g}} = -107$ meV, we obtain the following parameters: $J^{xx}_{12} = J^{yy}_{12} = 130.7$ meV and $J^{zz}_{12} = 131.6$ meV, which correspond to the out-of-plane configuration of the pseudospins ($J^{xx}_{12} = J^{yy}_{12} < J^{zz}_{12}$), being in total disagreement with the experimental situation [16].

This disagreement urged us, in addition to the hybridization, to consider another contribution to the t_{2g} level splitting, caused by the nonsphericity of the Madelung potential [26,48]. This term plays a crucial role in reproducing the correct magnetic ground state of $3d$ perovskite oxides with the partially filled t_{2g} shell [48,49]. It appears to be very important also for Ba_2IrO_4 because it reverses the order of the t_{2g} level ($\Delta^{\rm h+M}_{t_{2g}} = 69$ meV) and enforces the experimentally observed in-plane configuration of the pseudospins ($J^{xx}_{12} = J^{yy}_{12} > J^{zz}_{12}$). This is the reason why throughout this work we apply this strategy both for Ba_2IrO_4 and Sr_2IrO_4. For Ba_2IrO_4, it leads to the anisotropy of the g tensor, $g^{zz} > g^{xx} = g^{yy}$, which does not seem to be consistent with the prediction of Bogdanov *et al.* [34]. However, so far there are no experimental data for Ba_2IrO_4 and this situation still needs to be checked experimentally. As for Sr_2IrO_4, the anisotropy of the g tensor ($g^{xx} = 1.12$ and $g^{zz} = 3.33$) appears to be of the right sign, but, because of the large $\Delta^{\rm h+M}_{t_{2g}}$, is substantially overestimated in comparison with the experimental data [34]. Apparently, this problem is related to limitations of the low-energy model, which leads to the overestimation of the t_{2g} level splitting. Moreover, the numerical values can be to some extent corrected by employing more rigorous techniques for calculations of the g tensor [33,34], beyond the SE approximation.

We would also like to stress that, within the interval $\Delta^{\rm h}_{t_{2g}} < \Delta_{t_{2g}} < \Delta^{\rm h+M}_{t_{2g}}$, the DM interaction d^z_{12} in Sr_2IrO_4 only weakly depends on $\Delta_{t_{2g}}$. Thus, the small value of d^z_{12} and, therefore, the FM canting, obtained in our work, is not related to the t_{2g} level splitting, that also confirms the conclusions of Sec. V C. We also note that a smaller value of $\Delta_{t_{2g}}$ in the case of Sr_2IrO_4 would improve the agreement with the experimental

data for the g tensor (Ref. [34]) and also the values of NN exchange interactions in the xy plane (Refs. [41,42]) and the Néel temperature, which will be discussed in the next section. However, in the framework of the SE theory, it does not produce the longer-range exchange interactions in the xy plane, which are apparently suggested by the from of the experimental magnon dispersion [41,42]. Thus, simple change of the model parameters does not resolve all the problems of the SE description for Sr_2IrO_4.

E. Calculations of the Néel temperature

The first-principles calculations revealed a big difference of the magnetic models in the case of Ba_2IrO_4 and Sr_2IrO_4. On the one hand, the leading isotropic exchange interaction of 123 meV in Ba_2IrO_4 is about three times larger than that of 39 meV in Sr_2IrO_4. In turn, the symmetric anisotropic interaction $J_{12}^{(S)xy}$ in Ba_2IrO_4 is an order of magnitude larger than in Sr_2IrO_4. On the other hand, there is an appreciable DM interaction in Sr_2IrO_4, but not in Ba_2IrO_4. One of the puzzling points is that the experimental Néel temperature is practically the same in both systems (about 240 K). The aim of this section is to check whether such striking similarity can be explained using the above parameters of interatomic exchange interactions derived in the SE approximation.

Let us first investigate the effect of the DM interaction on the energy spectrum of the pseudospin model. In the $I4/mmm$ coordinate frame, the exchange interaction tensor in the bond 1-2, which is parallel to the y' axis, is given by

$$\overleftrightarrow{J}_{12} = \begin{pmatrix} J_{12}^{xx} - \Delta J_{12} & -d_{12}^{z} & 0 \\ d_{12}^{z} & J_{12}^{xx} + \Delta J_{12} & 0 \\ 0 & 0 & J_{12}^{zz} \end{pmatrix},$$

where for simplicity we have dropped the small contributions of d_{12}^{x} and d_{12}^{y}. For the bonds parallel to the x' axis, ΔJ_{12} should be replaced by $-\Delta J_{12}$. By considering the transformation

$$\overleftrightarrow{J}_{12} \to \overleftrightarrow{\tilde{J}}_{12} = \overleftrightarrow{U}_1 \overleftrightarrow{J}_{12} \overleftrightarrow{U}_2^{T}$$

with

$$\overleftrightarrow{U}_1 = \overleftrightarrow{U}_2^{T} = \begin{pmatrix} \cos\phi & \sin\phi & 0 \\ -\sin\phi & \cos\phi & 0 \\ 0 & 0 & 1 \end{pmatrix}$$

and $\phi = \frac{1}{2}\arctan(d_{12}^{z}/J_{12}^{xx})$ minimizing the energy of DM interactions [14,50], the tensor $\overleftrightarrow{J}_{12}$ can be transformed to

$$\overleftrightarrow{\tilde{J}}_{12} = \begin{pmatrix} \tilde{J}_{12}^{xx} - \Delta J_{12} & 0 & 0 \\ 0 & \tilde{J}_{12}^{xx} + \Delta J_{12} & 0 \\ 0 & 0 & J_{12}^{zz} \end{pmatrix},$$

where $\tilde{J}_{12}^{xx} = J_{12}^{xx}\sqrt{1 + (d_{12}^{z}/J_{12}^{xx})^2}$. Thus, the DM interactions alone do not confine the pseudospins in any particular directions [14,50]. Moreover, after such transformation to the local coordinate frame, the effect of the DM interactions can be combined with J_{12}^{xx}. Since in the six-orbital model for Sr_2IrO_4, $d_{12}^{z} = 3.97$ meV while $J_{12}^{xx} = 40.2$ meV, the renormalization of $\tilde{J}_{12}^{xx}$ due to the DM interaction is only about 0.5%. Therefore, we conclude that the effect of the DM interaction on the energy spectrum is small and can be neglected and, as far as the energy spectrum is concerned, the main ingredients of the pseudospin model are essentially the same in the case of Ba_2IrO_4 and Sr_2IrO_4.

We will concentrate on two mechanisms of the magnetic ordering in iridates: the first one is due to the in-plane anisotropy, which emerges in the six-orbital model, and the second one is due to the interlayer exchange coupling, which is relevant to the two-orbital model of Ba_2IrO_4. Thus, we consider the following general compass Heisenberg model:

$$\hat{\mathcal{H}}_{\mathcal{S}} = \frac{J_z}{2}\sum_{\langle ij\rangle \text{ in plane}} \mathcal{S}_i^z\mathcal{S}_j^z + \frac{1}{2}\sum_{\langle ij\rangle \| x}\left(J_\| \mathcal{S}_i^x\mathcal{S}_j^x + J_\perp \mathcal{S}_i^y\mathcal{S}_j^y\right) + \frac{1}{2}\sum_{\langle ij\rangle \| y}\left(J_\| \mathcal{S}_i^y\mathcal{S}_j^y + J_\perp \mathcal{S}_i^x\mathcal{S}_j^x\right) + \frac{J'}{2}\sum_{\langle ij\rangle \text{ interplane}} \boldsymbol{\mathcal{S}}_i\boldsymbol{\mathcal{S}}_j, \tag{6}$$

where it is convenient to introduce the shorthand notations $J_z \equiv J_{12}^{zz}$, $J_\| \equiv J_{12}^{xx} + \Delta J_{12}$, $J_\perp \equiv J_{12}^{xx} - \Delta J_{12}$, and J' is the coupling between the atoms, which belong to different planes, separated by the primitive translation c along the z axis. The magnon spectrum of this model for $J' = 0$ was calculated in Ref. [51]. It reads as

$$E_{\mathbf{q}}^{(1)} = \zeta S\sqrt{(4J_{\text{av}} + B_q - A_q)(4J_{\text{av}} + B_q + A_q + J_{\text{av}}g)},$$
$$E_{\mathbf{q}}^{(2)} = \zeta S\sqrt{(4J_{\text{av}} - B_q - A_q + J_{\text{av}}g)(4J_{\text{av}} - B_q + A_q)}, \tag{7}$$

where $J_{\text{av}} = (J_\| + J_\perp)/2 = J_{12}^{xx}$,

$$A_{\mathbf{q}} = (J_\perp + J_z)\cos q_x + (J_\| + J_z)\cos q_y,$$
$$B_{\mathbf{q}} = (J_\perp - J_z)\cos q_x + (J_\| - J_z)\cos q_y, \tag{8}$$

and

$$g = 0.16(J_\| - J_\perp)^2/\left(J_{\text{av}}^2 S\right) = 0.64\left(\Delta J_{12}/J_{12}^{xx}\right)^2/S \tag{9}$$

is the quantum gap. Moreover, we have introduced the renormalization factor $\zeta = 1 + 0.0785/S$, which is taken equal to its value in the two-dimensional Heisenberg model. Then, for small $\mathbf{q}$ we obtain

$$4J_{\text{av}} - B_{\mathbf{q}} - A_{\mathbf{q}} \to J_\perp q_x^2 + J_\| q_y^2,$$
$$4J_{\text{av}} - B_{\mathbf{q}} + A_{\mathbf{q}} \to 4(J_{\text{av}} + J_z),$$
$$4J_{\text{av}} + B_{\mathbf{q}} - A_{\mathbf{q}} \to 4(J_{\text{av}} - J_z) + J_z q^2 = J_z(q^2 + f),$$
$$4J_{\text{av}} + B_q + A_q \to 8J_{\text{av}}, \tag{10}$$

where the parameter f, describing the in-plane symmetric anisotropy, is defined as

$$f = 4(J_{\text{av}} - J_z)/J_z. \tag{11}$$

Therefore, we have

$$E_{\mathbf{q}}^{(1)} \simeq S\zeta\sqrt{8J_{\text{av}}J_z\left(q^2 + f\right)},$$
$$E_{\mathbf{q}}^{(2)} \simeq S\zeta\sqrt{4(J_{\text{av}} + J_z)\left(J_\perp q_x^2 + J_\| q_y^2 + J_{\text{av}}g\right)}. \tag{12}$$

The first mode is related to the out-of-plane pseudospin rotation, while the second corresponds to the in-plane rotation.

To obtain magnetic transition temperatures, we map the Heisenberg model (6) onto the nonlinear sigma model, having

TABLE I. Parameters used in Eqs. (13) and (14) for the transition temperature and the calculated T_N in different regimes (the values of $J_{\rm av}$, $J_\parallel - J_\perp$, and J_z are in meV, T_N is in Kelvin, and other parameters are dimensionless).

	$J_{\rm av}$	$J_\parallel - J_\perp$	J_z	f	g	α	$c_{\rm op}$	$c_{\rm ip}$	$T_N^{\alpha=0,g=0}$	T_N
Ba_2IrO_4 (2-orb.)	122.8	0	122.8	0	0	1.4×10^{-4}	200.9	200.9		239
Ba_2IrO_4 (6-orb.)	110.6	15	108.1	0.09	6×10^{-3}	1.3×10^{-4}	178.9	179.9	371	414
Sr_2IrO_4 (6-orb.)	40.2	1.5	36.7	0.38	4×10^{-4}	1.5×10^{-5}	62.8	64.3	181	216

the same excitation spectrum [Eq. (12)]. The details are given in the Appendix. Treating the magnetic excitations, as slightly different from the case of the XY anisotropy [52], we obtain in the regime $f \gg \max(\alpha, g), \alpha = 2J'/J$, the following equation for the Néel temperature (see Appendix):

$$T_N = 4\pi\rho_s \left\{ \ln \frac{T_N^2}{c_{\rm op} c_{\rm ip} f_r} + 4 \ln \frac{4\pi\rho_s}{T_N} - \frac{2A^2}{\ln^2[f/\max(\alpha,g)]} \right\}^{-1}, \tag{13}$$

where $A \simeq 3.5$, $c_{\rm op} = \sqrt{8 J_{\rm av} J_z} S\zeta$, and $c_{\rm ip} = \sqrt{4 J_{\rm av}(J_{\rm av} + J_z)} S\zeta$ are the out-of-plane and in-plane spin-wave velocities, $\rho_s = 2(1/\rho_z + 1/\rho_{\rm av})^{-1}$ is the effective spin stiffness ($\rho_{z,{\rm av}} = J_{z,{\rm av}} \zeta S \bar{S}_0$), $f_r = f(\bar{S}_0/S)^2$ is the renormalized anisotropy parameter, $\bar{S}_0 = 0.303$ for $S = \frac{1}{2}$ is the ground-state magnetization. In the absence of compass anisotropy, $f = g = 0$, we obtain instead [53]

$$T_N = 4\pi\rho_s \left\{ \ln \frac{2T_N^2}{c_{\rm op} c_{\rm ip} \alpha_r} + 3 \ln \frac{4\pi\rho_s}{T_N} - 0.06 \right\}^{-1}, \tag{14}$$

where $\alpha_r = \alpha(\bar{S}_0/S)$ is the renormalized interlayer coupling parameter.

The parameters and the resulting magnetic transition temperatures are listed in Table I. Let us first discuss the results of the six-orbital models for the Ba_2IrO_4 and Sr_2IrO_4. Judging by the ratio between the anisotropy parameters f, g and interlayer isotropic parameter α, we have the relation $f \gg g \gg \alpha$, which holds for both compounds. Thus, the in-plane anisotropy is expected to be mainly responsible for the magnetic ordering. The differences between in-plane and out-of-plane components of the symmetric anisotropy tensor ($J_{\rm av} - J_z$) are close to each other and equal to 2.5 meV (in Ba_2IrO_4) and 3.5 meV (in Sr_2IrO_4). However, due to the difference in the absolute value of J_z, we obtain completely different anisotropy parameters f, g and, therefore, the transition temperatures. For Sr_2IrO_4, the calculated temperature of 216 K is in the good agreement with the experimental value of 240 K. This is consistent with the finding of Jackeli and Khaliullin [14], who used the experimental T_N in order to estimate the values of the exchange interactions and these values are close to ours. However, the situation is different in the case of Ba_2IrO_4, where the theoretical T_N is overestimated by a factor of 2.

Interestingly, in the case of the two-orbital model for Ba_2IrO_4, which, in analogy with the cuprates [53], contains only in-plane and interplane isotropic exchange interactions, we observe a good agreement between theory and experiment. However, this agreement is probably fortuitous.

VI. BEYOND SUPEREXCHANGE

The main purpose of this section is to discuss the effects, which are not included to the regular SE model. Our main concern is the following: Since the SE model is based on the second-order perturbation theory for the transfer integrals, it implies that all effects of the SO coupling, which are included to these transfer integrals, are also automatically treated only up to the second order. Since the SO coupling is large in iridates, this may be a rather crude approximation, which does not take into account some important anisotropic interactions. For instance, in the mean-field approximation for the SE model, all pseudospins in the single xy plane of Ba_2IrO_4 and Sr_2IrO_4 can rotate rigidly at no energy cost. Aside from quantum effects, considered in the previous section (see also Ref. [17]), this may be related to the lack of the in-plane anisotropy, which typically appears only in the fourth order of the SO coupling.

If we wanted to include these effects in the pseudospin model, our strategy would be to go beyond the second-order perturbation theory for the transfer integrals and consider higher-order terms, which give rise to the new type of interactions, such as the biquadratic or ring exchange [54,55]. They will affect both anisotropic and isotropic parts of the exchange interactions. Therefore, in the pseudospin formulation, based on the strong SO coupling, these two types of the effects are connected with each other: if we want to consider the higher-order anisotropic interactions, we have to deal with the biquadratic and ring exchange terms, which will affect all other exchange interactions, including the isotropic ones. Such pseudopsin Hamiltonian is no longer presented in the bilinear form (3).

Nevertheless, in this work we take a different strategy and in order to evaluate the higher-order contributions (and, therefore, check the validity of the SE model) in Ba_2IrO_4 and Sr_2IrO_4, we solve the original electron model (1) in the mean-field HF approximation, where we also apply the staggered external magnetic field, which controls the directions of the spin and orbital moments. We have found that the field of $\mu_{\rm B} H = 0.68$ meV is generally sufficient for these purposes.

The weak point of the HF approach is that it treats all onsite electron-electron interactions on the mean-field level, whereas in the SE theory such processes are treated rigorously by solving the exact eigenstates problem for the virtual two-hole states. However, in this particular case, we do not expect large error caused by the mean-field approximation (some comparison for transition-metal perovskite oxides can be found in Ref. [26]). On the other hand, the HF method does not employ any additional approximations regarding the relative strength of transfer integrals and the onsite Coulomb repulsion and, in this sense, is the more superior approach in comparison with the SE theory.

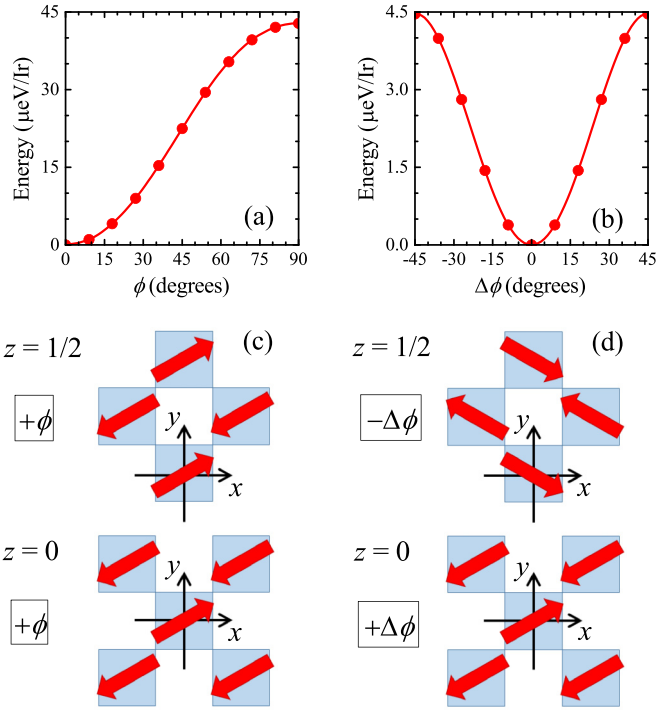

FIG. 8. (Color online) Results of constrained unrestricted Hartree-Fock calculations for Ba_2IrO_4 in the staggered "antiferromagnetic" field $\mu_B H = 0.68$ meV. The direction of the magnetic field in the planes $z = 0$ and $\frac{1}{2}$ is specified by azimuthal angles $(\phi + \Delta\phi)$ and $(\phi - \Delta\phi)$, respectively (in the $I4_1/acd$ coordinate frame). (a) The total energy dependence on ϕ for $\Delta\phi = 0$. (b) The total energy dependence on $\Delta\phi$ for $\phi = 0$. (c), (d) The geometry of the staggered magnetic field for (a) and (b), respectively.

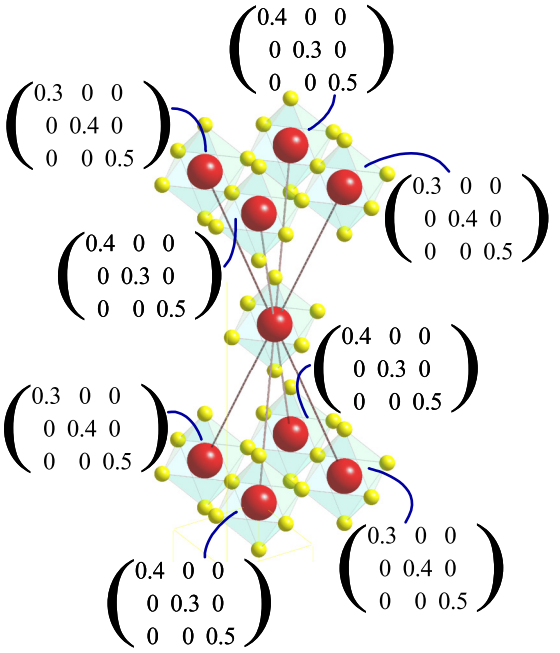

FIG. 9. (Color online) Tensors of superexchange interactions $\overleftrightarrow{J}_{ij}$ (in meV and in the $I4_1/acd$ coordinate frame), associated with different Ir-Ir bonds between adjacent planes in Ba_2IrO_4. The Ir atoms are indicated by the big (red) spheres and the oxygen atoms are indicated by the small (yellow) spheres.

Let us start with Ba_2IrO_4. The geometry of the constraining field in this case is explained in Fig. 8. First, let us consider the case where the fields in the two adjacent planes $z = 0$ and $\frac{1}{2}$ are rotated in phase. Then, the total energy exhibits the minimum at $\phi = 0$ (modulo π, in the $I4_1/acd$ coordinate frame). This effect can be actually included in the SE model and is related to the anisotropy of the exchange interactions between adjacent planes [17]. The behavior of these interactions is explained in Fig. 9. Then, the mean-field energy of the magnetic order, depicted in Fig. 8(c), is given by $E(\phi) = -\Delta J_{\text{out}} \cos 2\phi$ (per one Ir site), where $\Delta J_{\text{out}} = |J^{xx}_{\text{out}} - J^{yy}_{\text{out}}|$.

Furthermore, in the SE approximation, the energy should remain invariant with respect to the antiphase rotations of the pseudospin [Fig. 8(d)]. In other words, if we fix ϕ and consider the configurations, where the directions of the pseudospins in the adjacent planes $z = 0$ and $\frac{1}{2}$ are specified by the azimuthal angles $(\phi + \Delta\phi)$ and $(\phi - \Delta\phi)$, respectively, the mean-field energy of such configurations should not depend on $\Delta\phi$ [17]. This property is indeed strictly observed when we use the exchange parameters, derived in the SE model. Because of this degeneracy, the authors of Ref. [17] had to go beyond the mean-field theory and consider the effect of the quantum fluctuations in order to explain the experimentally observed magnetic ground-state structure of Ba_2IrO_4 (corresponding to $\phi = \Delta\phi = 0$ in the $I4_1/acd$ coordinate frame) [16]. The most interesting aspect of our analysis is that this degeneracy can be lifted even on the mean-field level if one goes beyond the SE model and consider more rigorously the higher-order contributions of the transfer integrals in the framework of the unrestricted HF calculations. The dependence of the HF total energy on $\Delta\phi$ is shown in Fig. 8(b) (for $\phi = 0$). It clearly shows that the higher-order anisotropic interactions, which are included in the HF calculations, lift the degeneracy and stabilize the experimentally observed magnetic ground state. The energy barrier, caused by these interactions, is about 4.5 μeV, which is at least comparable with the effect of quantum fluctuations considered in Ref. [17]. Thus, the effect is robust and cannot be neglected in the realistic analysis of the magnetic properties of Ba_2IrO_4.

Next, we evaluate the effect of biquadratic exchange on the NN interaction J^{zz}_{12} in the xy plane of Ba_2IrO_4. If the magnetic properties of some material were indeed described by the bilinear Hamiltonian (3), the values of the exchange parameters would not depend on the method, which is used for their calculations. For instance, in the mean-field HF method, one could evaluate J^{zz}_{12} from the total energy difference between FM and AFM states, by aligning the magnetic moments parallel to the z axis: $J^{zz}_{12} = E_{\uparrow\uparrow} - E_{\uparrow\downarrow}$. Then, if the bilinear parametrization (3) for the magnetic Hamiltonian were indeed appropriate, this value of J^{zz}_{12} should be close to the one obtained in the SE model. Nevertheless, the straightforward HF calculations yield $E_{\uparrow\uparrow} - E_{\uparrow\downarrow} = 83.8$ meV, which is 22% smaller than $J^{zz}_{12} = 108.1$ meV, obtained in the SE model. This deviation is the measure of biquadratic (or ring-type) exchange interactions, existing in the system. Thus, as expected from the discussion in the beginning of this section, the higher-order anisotropic effects in Ba_2IrO_4 coexist with

appreciable biquadratic contributions to the isotropic exchange interaction. In this sense, we obtain very consistent description for Ba_2IrO_4. Unfortunately, we could not obtain a stable in-plane FM solution in the HF method and, thus, evaluate the in-plane elements of the exchange tensor from the total energy difference. Generally, one can expect similar contribution of biquadratic interactions to the in-plane and out-of-plane components of the exchange tensor.

The behavior of Sr_2IrO_4 appears to be rather different from Ba_2IrO_4. Since the transfer integrals are smaller in Sr_2IrO_4, while the Coulomb interactions are slightly larger, it is reasonable to expect that the t_{2g} states are more localized in Sr_2IrO_4, which additionally justifies the use of the SE model. This is indeed what we have obtained by comparing results of HF calculations and the SE model. The fact that Ba_2IrO_4 appears to be "more itinerant" than Sr_2IrO_4 can be seen already from the comparison of the band gap, obtained in the HF method for the AFM ground state, which is substantially smaller in Ba_2IrO_4 (1.3 eV, against 1.8 eV in Sr_2IrO_4). It should be noted, however, that the HF gap is considerably larger than the experimental one, due to the lack of quantum and thermal fluctuations, as was confirmed by the DMFT calculations [15].

First, we consider the HF solutions for the FM and AFM states, where all magnetic moments are parallel to the z axis. The exchange coupling obtained from the total energy difference between these states is 31.7 meV, which is much closer to the value $J_{12}^{zz} = 36.7$ meV, obtained in the SE model (the difference is about 14%, which can be again regarded as the measure of biquadratic interactions in the system). In Sr_2IrO_4, it is practically impossible to evaluate the in-plane elements of the exchange tensor from the total energy difference: because of the DM interaction, the in-plane FM state is unstable and converges to the AFM state (with the small FM canting of the magnetic moments).

Next, we consider the higher-order anisotropy effects in Sr_2IrO_4. For these purposes we take the weakly FM state and rotate magnetic moments by the external magnetic field of $\mu_B H = 0.68$ meV, which couples to the weak FM moment in the xy plane. The results of such constrained HF calculations are summarized in Fig. 10. We note the following: (i) The total energy depends on the direction of the magnetic moments in the xy plane. However, this dependence is very weak (the characteristic energy barrier is about 0.25 meV, which is an order of magnitude smaller than in Ba_2IrO_4). (ii) The angle ($\Delta\phi$) between magnetic moments of the sites 2 and 1 (see Fig. 1 for the notations) is nearly constant, meaning that it is mainly controlled by the DM interaction d_{12}^z, while the effect of other anisotropic interactions (that are not taken into account in the SE model) are relatively small. Since the energy gain caused by the DM interaction is proportional to $d_{12}^z \sin\Delta\phi$, the obtained values of $-270^\circ < \Delta\phi < -180^\circ$ are well consistent with the sign $d_{12}^z < 0$ of DM interactions for the counterclockwise rotation of the IrO_6 octahedra around the site 1 (see Fig. 1). Yet, one interesting aspect of the HF analysis is that the angle $\Delta\phi$ is different between, separately, spin and orbital magnetic moments. Without external field ($H = 0$), $\Delta\phi$ is about -185.2°. It corresponds to the FM canting of 2.6°, which is close to 2.8°, obtained in the SE model. The values of spin and orbital magnetic moments, obtained for the in-plane

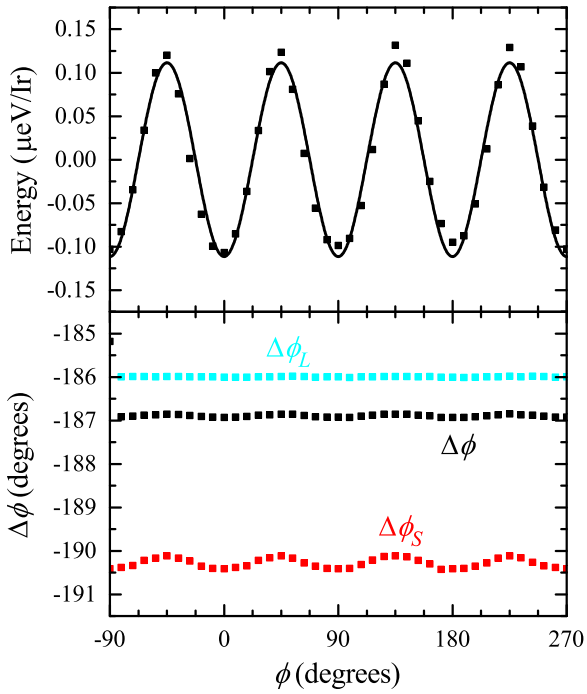

FIG. 10. (Color online) Results of constrained unrestricted Hartree-Fock calculations for Sr_2IrO_4 in the magnetic field $\mu_B H = 0.68$ meV, which couples to the weak ferromagnetic moment in the xy plane. The direction of the field is specified by the azimuthal angle ϕ. The upper panel displays the behavior of the total energy: the symbols show calculated points, while the solid line is the result of interpolation $E(\phi) = A + B\cos 4\phi$. The lower panel shows the angle between spin ($\Delta\phi_S$), orbital ($\Delta\phi_L$), and total ($\Delta\phi$) magnetic moments of the sites 2 and 1 in Fig. 1.

(out-of-plane) magnetic alignment are 0.13 and 0.48 μ_B (0.71 and 0.83 μ_B), respectively.

Thus, we obtain a very consistent description also for Sr_2IrO_4: (i) To a good approximation, the magnetic Hamiltonian has the bilinear form (3), inherent to the SE model. (ii) The higher-order anisotropy effects, beyond the SE model, are negligibly small. This makes the main difference from Ba_2IrO_4, where (i) the deviations from the bilinear form are significant and (ii) the higher-order anisotropic exchange interactions are important.

VII. SUMMARY AND CONCLUSIONS

The main purpose of this work was to critically evaluate the abilities of the SE model for the analysis of magnetic properties of the layered iridates Ba_2IrO_4 and Sr_2IrO_4. Being based on the DFT calculations with the SO coupling, we have first derived the effective low-energy electron model for the t_{2g} bands, which are located near the Fermi level and primarily responsible for the magnetic properties of Ba_2IrO_4 and Sr_2IrO_4. This electron model was further mapped on the pseudospin model using the theory of SE interactions in the limit of large onsite Coulomb repulsion. We have studied the microscopic origin of the bond-dependent anisotropic exchange interactions, as well as the antisymmetric DM interactions, caused by the antiphase rotations of the IrO_6

octahedra in Sr_2IrO_4. The pseudospin Hamiltonian problem has been solved by means of the nonlinear sigma model, that has finally allowed us to evaluate the Néel temperature. We have demonstrated that while for Sr_2IrO_4 the theoretical Néel temperature is in good agreement with the experimental data, for Ba_2IrO_4 it is overestimated by factor of 2. We have argued that this discrepancy is consistent with the limitations of the SE model for Ba_2IrO_4, which is the more "itinerant" system than Sr_2IrO_4. Such "itineracy" is directly related to the details of the electronic structure of Ba_2IrO_4: the lack of rotations of the IrO_6 octahedra and the proximity of the Ba $5d$ states to the Fermi level make the t_{2g} bandwidth increase and more efficiently screen the Coulomb interactions in this band. Thus, the $\hat{t}/\mathcal{U}$ expansion for the magnetic energy converges slower, and higher-order terms, beyond the SE contributions, start to play an important role. Since the effect of SO interaction in the SE formulation is included to the transfer integrals, the higher-order terms automatically improve the description also for the anisotropic exchange interactions. In fact, by solving the low-energy electron model for Ba_2IrO_4 in the HF approximation, we were able to reproduce the experimental magnetic-ground-state structure of this compound even on the mean-field level, without invoking quantum effects. Another important problem, which deserves further consideration, is the contribution of the oxygen states to the interatomic exchange interactions.

ACKNOWLEDGMENTS

We acknowledge fruitful communication with A. Tsirlin. This work is partly supported by the grant of Russian Science Foundation (Project No. 14-12-00306).

APPENDIX: DERIVATION OF THE NONLINEAR SIGMA MODEL FOR COMPASS HEISENBERG MODEL AND ITS RENORMALIZATION

1. Nonlinear sigma model

To obtain the action of the continuum model we pass to the coherent state representation for spin operators and represent the corresponding vectors of spin directions following the standard procedure

$$\boldsymbol{\mathcal{S}}_i = (-1)^i S\mathbf{n}_i\sqrt{1-(\mathbf{L}_i/S)^2} + \mathbf{L}_i, \tag{A1}$$

where $\mathbf{L}_i \cdot \mathbf{n}_i = 0$, $\mathbf{n}_i^2 = 1$, and the fields $\mathbf{n}_i$ and $\mathbf{L}_i$ represent the staggered and uniform component. Substituting Eq. (A1) into (6) we obtain the Lagrangian

$$\begin{aligned} L[\mathbf{n},\mathbf{L}] = &-\frac{J_z S^2}{2}\sum_{i,\delta} n_i^z n_{i+\delta}^z - \frac{S^2}{2}\sum_{i,\delta_x}\left(J_\parallel n_i^x n_{i+\delta_x}^x + J_\perp n_i^y n_{i+\delta_x}^y\right) - \frac{S^2}{2}\sum_{i,\delta_y}\left(J_\parallel n_i^y n_{i+\delta_y}^y + J_\perp n_i^x n_{i+\delta_y}^x\right) \\ &+ \frac{1}{2}\sum_{i,\delta}\left(J_z L_i^z L_{i+\delta}^z + \left(J_z n_z^2 + J_\parallel n_\delta^2 + J_\perp n_{\tilde{\delta}}^2\right)\frac{\mathbf{L}_i^2 + \mathbf{L}_{i+\delta}^2}{2}\right) + \frac{1}{2}\sum_{i,\delta_x}\left(J_\parallel L_i^x L_{i+\delta_x}^x + J_\perp L_i^y L_{i+\delta_x}^y\right) \\ &+ \frac{1}{2}\sum_{i,\delta_y}\left(J_\parallel L_i^y L_{i+\delta_y}^y + J_\perp L_i^x L_{i+\delta_y}^x\right) + i\sum_i \mathbf{L}_i\cdot[\mathbf{n}_i\times\partial_\tau\mathbf{n}_i], \end{aligned} \tag{A2}$$

where $\delta_{x,y}$ correspond to nearest neighbours along x and y directions, $n_{\delta_{x,y}} = n_{x,y}$, $n_{\tilde{\delta}_{x,y}} = n_{y,x}$, and we keep only terms, which give the leading contribution in the continuum limit. Expanding

$$\mathbf{n}_{i+\delta} = \mathbf{n}_i + (\delta\nabla)\mathbf{n}_i + \tfrac{1}{2}(\delta^a\delta^b\partial_a\partial_b)\mathbf{n}_i + \ldots \tag{A3}$$

and similarly for $\mathbf{L}_{i+\delta}$, we obtain

$$\begin{aligned} L[\mathbf{n},\mathbf{L}] = &\frac{S^2}{2}\int d^2\mathbf{x}\left[J_z(\nabla n_z)^2 + J_\parallel(\partial_x n_x)^2 + J_\parallel(\partial_y n_y)^2 + J_\perp(\partial_x n_y)^2 + J_\perp(\partial_y n_x)^2 + J_z f n_z^2\right] \\ &+ \frac{1}{2}\int d^2\mathbf{x}\left\{2\left[4J_z + (J_\parallel + J_\perp - 2J_z)\left(n_x^2 + n_y^2\right)\right]\mathbf{L}_i^2 + 2(J_\parallel + J_\perp - 2J_z)\left(L_x^2 + L_y^2\right)\right\} + i\mathbf{L}\cdot[\mathbf{n}\times\partial_\tau\mathbf{n}], \end{aligned} \tag{A4}$$

where we have defined f according to (11). Performing the integration over $\mathbf{L}$, we find

$$\begin{aligned} L[\mathbf{n}] = &\frac{S^2}{2}\int d^2\mathbf{x}\left[J_z(\nabla n_z)^2 + J_\parallel(\partial_x n_x)^2 + J_\parallel(\partial_y n_y)^2 + J_\perp(\partial_x n_y)^2 + J_\perp(\partial_y n_x)^2 + J_z f n_z^2\right] \\ &+ \frac{1}{2}\int d^2\mathbf{x}\frac{1}{2\left[4J_z + (J_\parallel + J_\perp - 2J_z)\left(n_x^2 + n_y^2\right)\right]}[\mathbf{n}\times\partial_\tau\mathbf{n}]_z^2 + \frac{1}{2}\int d^2\mathbf{x}\frac{1}{2\left[4J_z + (J_\parallel + J_\perp - 2J_z)\left(1 + n_x^2 + n_y^2\right)\right]} \\ &\times [\mathbf{n}\times\partial_\tau\mathbf{n}]_x^2 + \frac{1}{2}\int d^2\mathbf{x}\frac{1}{2\left[4J_z + (J_\parallel + J_\perp - 2J_z)\left(1 + n_x^2 + n_y^2\right)\right]}[\mathbf{n}\times\partial_\tau\mathbf{n}]_y^2. \end{aligned} \tag{A5}$$

In the following, we assume the preferable direction of magnetic order along the y axis. Representing

$$n_y = \sqrt{1 - n_x^2 - n_z^2} \tag{A6}$$

and expanding in $n_{x,z}$ we obtain two branches of the magnon spectrum

$$\begin{aligned} E_z^2 &= 4S^2 J_z (J_\parallel + J_\perp)(q^2 + f), \\ E_x^2 &= 2S^2 (2J_z + J_\parallel + J_\perp)\big(J_\parallel q_x^2 + J_\perp q_y^2\big), \end{aligned} \tag{A7}$$

which coincides with small-q expansion of the results of Sec. V E and Ref. [51].

2. Perturbation theory

In the following, we concentrate on the classical part of the Lagrangian (A5), renormalized by the quantum fluctuations

$$L_{\rm cl}[\mathbf{n}] = \frac{1}{2}\int d^2\mathbf{x}\big\{\rho_r\big[(\nabla n_z)^2 + f_r n_z^2\big] + \rho_\parallel\big[(\partial_x n_x)^2 + (\partial_y n_y)^2\big] + \rho_\perp\big[(\partial_x n_y)^2 + (\partial_y n_x)^2\big]\big\}. \tag{A8}$$

In Eq. (A8), we use the quantum-renormalized spin stiffnesses $\rho_r = J_z S\overline{S}_0\zeta$ and $\rho_{\parallel,\perp} = J_{\parallel,\perp} S\overline{S}_0\zeta$, where $\overline{S}_0 = S - 0.197$ is the ground-state magnetization of the square-lattice Heisenberg model, $\zeta = 1 + 0.157/(2S)$ is the exchange parameter renormalization factor, the bare spin stiffnesses anisotropy, and the renormalized easy-plane anisotropy $f_r = f\overline{S}_0^2/(S\zeta)^2$. Following the standard procedure [52,56], we assume that the excitations, described by $L_{\rm cl}[\mathbf{n}]$ are cut on the ultraviolet at the momentum $\Lambda_{\rm uv} = T/c$, where $c = \sqrt{8}JS\zeta$ is the renormalized spin-wave velocity; the remaining (nonuniversal) contribution of the other part of momentum space yields the above-mentioned quantum renormalizations.

Assuming again the long-range order along the y axis, introducing $\boldsymbol{\pi} = (n_x, n_z)$, and using Eq. (A6), we obtain

$$\begin{aligned} L_{\rm cl}[\mathbf{n}] = \frac{1}{2}\int d^2\mathbf{x}\Big\{\rho_r\big[(\nabla\pi_z)^2 + f_r\pi_z^2\big] + \rho_\parallel(\partial_x\pi_x)^2 + \rho_\perp(\partial_y\pi_x)^2 + \frac{\rho_\parallel}{1-\boldsymbol{\pi}^2}(\boldsymbol{\pi}\partial_y\boldsymbol{\pi})^2 + \frac{\rho_\perp}{1-\boldsymbol{\pi}^2}(\boldsymbol{\pi}\partial_x\boldsymbol{\pi})^2\Big\} \\ + \frac{T}{2}\int d^2\mathbf{x}\ln(1-\boldsymbol{\pi}^2) - h\int d^2\mathbf{x}\sqrt{1-\boldsymbol{\pi}^2}, \end{aligned} \tag{A9}$$

where the first term in the second line comes from the integration measure and in the last term we have introduced external magnetic field along the y axis, which will be set to 0 in the end. To perform renormalization of Eq. (A9), we decouple the interactions via the Wick theorem

$$\begin{aligned} L_{\rm cl}[\mathbf{n}] =& \frac{1}{2}\int d^2\mathbf{x}\big\{\rho_r\big[(\nabla\pi_z)^2 + f_r\pi_z^2\big] + \rho_\parallel(\partial_x\pi_x)^2 + \rho_\perp(\partial_y\pi_x)^2 + \rho_\parallel\langle\pi_a^2\rangle(\partial_y\pi_a)^2 + \rho_\perp\langle\pi_a^2\rangle(\partial_x\pi_a)^2 + \rho_\parallel\langle(\partial_y\pi_a)^2\rangle\pi_a^2 \\ &+ \rho_\perp\langle(\partial_x\pi_a)^2\rangle\pi_a^2\big]\big\} + \frac{1}{2}\int d^2\mathbf{x}\Big[h\boldsymbol{\pi}^2 + \frac{h}{2}\big(3\langle\pi_x^2\rangle + \langle\pi_z^2\rangle\big)\pi_x^2 + \frac{h}{2}\big(3\langle\pi_z^2\rangle + \langle\pi_x^2\rangle\big)\pi_z^2 - T\boldsymbol{\pi}^2\Big]. \end{aligned} \tag{A10}$$

Rescaling the fields

$$\pi_x \to Z_x\pi_x, \quad \pi_z \to Z_z\pi_z,$$

we obtain renormalized parameters

$$\begin{aligned} \rho_R &= Z_z^2\big[\rho_r + \rho_{xy}\langle\pi_z^2\rangle\big], \\ \rho_{\parallel R} &= Z_x^2\big[\rho_\parallel + \rho_\perp\langle\pi_x^2\rangle\big], \\ \rho_{\perp R} &= Z_x^2\big[\rho_\perp + \rho_\parallel\langle\pi_x^2\rangle\big], \\ \rho_R f_R + h_R &= Z_z^2\Big[h + \rho_r f_r + T\int\frac{d^2q}{(2\pi)^2}\frac{\rho_\parallel q_y^2 + \rho_\perp q_x^2}{\rho_r(q^2+f_r)+h} - T + \frac{h}{2}\big(3\langle\pi_z^2\rangle + \langle\pi_x^2\rangle\big)\Big], \\ \rho_{xy,R} g_R + h_R &= Z_x^2\Big[h + T\int\frac{d^2q}{(2\pi)^2}\frac{\rho_\parallel q_y^2 + \rho_\perp q_x^2}{\rho_\parallel q_x^2 + \rho_\perp q_y^2 + \rho_{xy} g + h} - T + \frac{h}{2}\big(3\langle\pi_x^2\rangle + \langle\pi_z^2\rangle\big)\Big], \end{aligned} \tag{A11}$$

where $\rho_{xy} = (\rho_\parallel + \rho_\perp)/2$,

$$\begin{aligned} \langle\pi_z{}^2\rangle &= T\int\frac{d^2q}{(2\pi)^2}\frac{1}{\rho_r(q^2+f_r)+h}, \\ \langle\pi_x{}^2\rangle &= T\int\frac{d^2q}{(2\pi)^2}\frac{1}{\rho_\parallel q_x^2 + \rho_\perp q_y^2 + \rho_{xy} g + h}, \end{aligned} \tag{A12}$$

and g_R is the gap, generated for π_x mode, which also contains the nonuniversal bare value g, determined by Eq. (9). From Eqs. (A11) we obtain

$$\begin{aligned} Z_x &= Z_z = Z, \\ h_R &= Z^2 h\big[1 + \tfrac{1}{2}\big(\langle\pi_z^2\rangle + \langle\pi_x^2\rangle\big)\big], \\ \rho_R f_R &= \rho_r Z^2 f_r\big[1 - \langle\pi_z^2\rangle\big], \\ \rho_{xy,R} g_R &= \rho_{xy,r} Z^2 g\big[1 - \langle\pi_x^2\rangle\big]. \end{aligned} \tag{A13}$$

Finally, Z is fixed by the condition that π_y renormalizes the same way, as π_x, which is due to 90° rotation symmetry in the plane. This implies $h_R = Zh$, such that

$$\begin{aligned} Z &= 1 - \tfrac{1}{2}\big(\langle\pi_z^2\rangle + \langle\pi_x^2\rangle\big), \\ \rho_R &\approx \rho_r\big[1 - \langle\pi_x^2\rangle\big], \\ f_R &\approx f_r\big[1 - 2\langle\pi_z^2\rangle\big], \\ \rho_{xy,R}/\rho_{xy} &= 1 - \langle\pi_z^2\rangle, \\ \gamma_R/\gamma &= g_R/g = 1 - 2\langle\pi_x^2\rangle, \end{aligned} \tag{A14}$$

where we have introduced $\gamma = (\rho_\parallel - \rho_\perp)/(2\rho_{xy})$ and neglected small anisotropy terms in the second and third lines. Being rewritten through these quantities, the effective Lagrangian reads as

$$\begin{aligned} L_R[\mathbf{n}] = &\frac{1}{2}\int d^2\mathbf{x}\Big\{\rho_R\big[(\nabla\pi_z)^2 + f_r\pi_z^2\big] + \rho_{xy,R}[(\nabla\pi_x)^2 + g_R + \gamma_R(\partial_x\pi_x)^2 - \gamma_R(\partial_y\pi_x)^2] + \frac{\rho_{xy,R}}{1-\boldsymbol{\pi}^2}(\boldsymbol{\pi}\nabla\boldsymbol{\pi})^2 \\ &+ \frac{\rho_{xy,R}\gamma_R}{1-\boldsymbol{\pi}^2}[(\boldsymbol{\pi}\partial_x\boldsymbol{\pi})^2 - (\boldsymbol{\pi}\partial_y\boldsymbol{\pi})^2]\Big\}. \end{aligned} \tag{A15}$$

3. Renormalization group

To perform renormalization group (RG) analysis, we introduce sharp momentum cutoff at scale Λ and vary Λ from $\Lambda_{\rm uv}$ to the smallest possible scale; in the following, we replace accordingly the index R at the renormalized quantities by Λ, denoting explicitly at which infrared scale they are evaluated. We also assume in the following that $f > g > \alpha$. According to the obtained expressions, we perform renormalization group procedure in two steps. At the first step, we integrate degrees of freedom at momenta scales $f_\Lambda^{1/2} < \Lambda < \Lambda_{\rm uv}$. In this range we can neglect small difference between x and z modes in Eqs. (A14) and obtain the standard flow equations of the $O(3)$ nonlinear sigma model with small easy-plane anisotropy

$$\begin{aligned} \frac{dt_\Lambda}{d\ln(1/\Lambda)} &= t_\Lambda^2 + t_\Lambda^3, \\ \frac{d\ln Z_\Lambda}{d\ln(1/\Lambda)} &= -t_\Lambda, \\ \frac{d\ln g_\Lambda}{d\ln(1/\Lambda)} &= \frac{d\ln\gamma_\Lambda}{d\ln(1/\Lambda)} = \frac{d\ln f_\Lambda}{d\ln(1/\Lambda)} = -2t_\Lambda, \end{aligned} \tag{A16}$$

where $t_\Lambda = T/(2\pi\rho_\Lambda)$. In the first equation of (A16) we have added the two-loop term of the $O(3)$ model. The solution of Eqs. (A16) is well known:

$$\begin{aligned} t_\Lambda &= \frac{t_r}{1 - t_r\ln\left(\frac{\Lambda_{\rm uv}t_\Lambda}{\Lambda t_r}\right)}, \\ Z_\Lambda &= \frac{t_r}{t_\Lambda} = 1 - t_r\ln\left(\frac{\Lambda_{\rm uv}t_\Lambda}{\Lambda t_r}\right), \\ \frac{g_\Lambda}{g_r} &= \frac{\gamma_\Lambda}{\gamma} = \frac{f_\Lambda}{f_r} = \left(\frac{t_r}{t_\Lambda}\right)^2 = \left[1 - t_r\ln\left(\frac{\Lambda_{\rm uv}t_\Lambda}{\Lambda t_r}\right)\right]^2, \end{aligned} \tag{A17}$$

where we have introduced $t_r = T/(2\pi\rho_r)$. The scaling is stopped at $\Lambda = \Lambda_f$, which fulfills $f_{\Lambda_f} = \Lambda_f^2$. The condition $t_{\Lambda_f} = 1$ determines the Kosterlitz-Thouless temperature in the absence of the in-plane anisotropy. At the scales $g_\Lambda^{1/2} < \Lambda < f_\Lambda^{1/2}$, the z

mode is fully gapped, and we obtain behavior of the coupling constants

$$\frac{dt_{xy,\Lambda}}{d\ln(1/\Lambda)} = \frac{d\ln f_\Lambda}{d\ln(1/\Lambda)} = 0, \quad \frac{d\ln Z_\Lambda}{d\ln(1/\Lambda)} = -t_{xy,\Lambda}/2, \quad \frac{d\ln g_\Lambda}{d\ln(1/\Lambda)} = \frac{d\ln \gamma_\Lambda}{d\ln(1/\Lambda)} = -2t_{xy,\Lambda}, \tag{A18}$$

which is in the XY universality class. The consideration of this regime is similar to the case of quasi-two-dimensional easy-plane model [52] and yields the result for the Néel temperature in Eq. (13) of the main text.

[1] G. Cao, J. Bolivar, S. McCall, J. E. Crow, and R. P. Guertin, Phys. Rev. B **57**, R11039 (1998).
[2] B. J. Kim, H. Jin, S. J. Moon, J.-Y. Kim, B.-G. Park, C. S. Leem, J. Yu, T. W. Noh, C. Kim, S.-J. Oh, J.-H. Park, V. Durairaj, G. Cao, and E. Rotenberg, Phys. Rev. Lett. **101**, 076402 (2008).
[3] B. J. Kim, H. Ohsumi, T. Komesu, S. Sakai, T. Morita, H. Takagi, and T. Arima, Science **323**, 1329 (2009).
[4] S. Nakatsuji, Y. Machida, Y. Maeno, T. Tayama, T. Sakakibara, J. van Duijn, L. Balicas, J. N. Millican, R. T. Macaluso, and J. Y. Chan, Phys. Rev. Lett. **96**, 087204 (2006).
[5] Y. Okamoto, M. Nohara, H. Aruga-Katori, and H. Takagi, Phys. Rev. Lett. **99**, 137207 (2007).
[6] G. Chen and L. Balents, Phys. Rev. B **78**, 094403 (2008).
[7] X. Wan, A. M. Turner, A. Vishwanath, and S. Y. Savrasov, Phys. Rev. B **83**, 205101 (2011).
[8] X. Liu, T. Berlijn, W.-G. Yin, W. Ku, A. Tsvelik, Y.-J. Kim, H. Gretarsson, Y. Singh, P. Gegenwart, and J. P. Hill, Phys. Rev. B **83**, 220403(R) (2011).
[9] S. K. Choi, R. Coldea, A. N. Kolmogorov, T. Lancaster, I. I. Mazin, S. J. Blundell, P. G. Radaelli, Y. Singh, P. Gegenwart, K. R. Choi, S.-W. Cheong, P. J. Baker, C. Stock, and J. Taylor, Phys. Rev. Lett. **108**, 127204 (2012).
[10] A. Biffin, R. D. Johnson, S. Choi, F. Freund, S. Manni, A. Bombardi, P. Manuel, P. Gegenwart, and R. Coldea, Phys. Rev. B **90**, 205116 (2014).
[11] T. Takayama, A. Kato, R. Dinnebier, J. Nuss, H. Kono, L. S. I. Veiga, G. Fabbris, D. Haskel, and H. Takagi, Phys. Rev. Lett. **114**, 077202 (2015).
[12] A. Kitaev, Ann. Phys. (NY) **321**, 2 (2006).
[13] P. W. Anderson, Phys. Rev. **115**, 2 (1959).
[14] G. Jackeli and G. Khaliullin, Phys. Rev. Lett. **102**, 017205 (2009).
[15] R. Arita, J. Kuneš, A. V. Kozhevnikov, A. G. Eguiluz, and M. Imada, Phys. Rev. Lett. **108**, 086403 (2012).
[16] S. Boseggia, R. Springell, H. C. Walker, H. M. Rønnow, Ch. Rüegg, H. Okabe, M. Isobe, R. S. Perry, S. P. Collins, and D. F. McMorrow, Phys. Rev. Lett. **110**, 117207 (2013).
[17] V. M. Katukuri, V. Yushankhai, L. Siurakshina, J. van den Brink, L. Hozoi, and I. Rousochatzakis, Phys. Rev. X **4**, 021051 (2014).
[18] H. Jin, H. Jeong, T. Ozaki, and J. Yu, Phys. Rev. B **80**, 075112 (2009).
[19] B. H. Kim, G. Khaliullin, and B. I. Min, Phys. Rev. Lett. **109**, 167205 (2012).
[20] J. I. Igarashi and T. Nagao, Phys. Rev. B **88**, 104406 (2013).
[21] N. B. Perkins, Y. Sizyuk, and P. Wölfle, Phys. Rev. B **89**, 035143 (2014).
[22] H. Okabe, M. Isobe, E. Takayama-Muromachi, A. Koda, S. Takeshita, M. Hiraishi, M. Miyazaki, R. Kadono, Y. Miyake, and J. Akimitsu, Phys. Rev. B **83**, 155118 (2011).
[23] M. K. Crawford, M. A. Subramanian, R. L. Harlow, J. A. Fernandez-Baca, Z. R. Wang, and D. C. Johnston, Phys. Rev. B **49**, 9198 (1994).
[24] N. E. Christensen, Int. J. Quantum Chem. **25**, 233 (1984).
[25] O. K. Andersen, Phys. Rev. B **12**, 3060 (1975); O. Gunnarsson, O. Jepsen, and O. K. Andersen, *ibid.* **27**, 7144 (1983); O. K. Andersen, Z. Pawlowska, and O. Jepsen, *ibid.* **34**, 5253 (1986).
[26] I. V. Solovyev, J. Phys.: Condens. Matter **20**, 293201 (2008).
[27] N. Marzari and D. Vanderbilt, Phys. Rev. B **56**, 12847 (1997).
[28] I. V. Solovyev, Z. V. Pchelkina, and V. I. Anisimov, Phys. Rev. B **75**, 045110 (2007).
[29] L. Hedin, Phys. Rev. **139**, A796 (1965); F. Aryasetiawan and O. Gunnarsson, Rep. Prog. Phys. **61**, 237 (1998).
[30] F. Aryasetiawan, M. Imada, A. Georges, G. Kotliar, S. Biermann, and A. I. Lichtenstein, Phys. Rev. B **70**, 195104 (2004).
[31] I. V. Solovyev, New J. Phys. **11**, 093003 (2009).
[32] N. W. Ashcroft and N. D. Mermin, *Solid State Physics* (Holt, Rinehart and Winston, Austin, TX, 1976).
[33] H. Bolvin, Chem. Phys. Chem. **7**, 1575 (2006); S. Vancoillie, P.-Å. Malmqvist, and K. Pierloot, *ibid.* **8**, 1803 (2007).
[34] N. A. Bogdanov, V. M. Katukuri, J. Romhányi, V. Yushankhai, V. Kataev, B. Büchner, J. van den Brink, and L. Hozoi, Nat. Commun. **6**, 7306 (2016).
[35] All parameters of the model Hamiltonian are available upon request.
[36] A. M. Oleś, G. Khaliullin, P. Horsch, and L. F. Feiner, Phys. Rev. B **72**, 214431 (2005).
[37] J. Kanamori, Prog. Theor. Phys. **30**, 275 (1963).
[38] I. V. Solovyev, I. V. Kashin, and V. V. Mazurenko, Phys. Rev. B **92**, 144407 (2015).
[39] I. V. Solovyev, Phys. Rev. Lett. **95**, 267205 (2005).
[40] L. Vaugier, H. Jiang, and S. Biermann, Phys. Rev. B **86**, 165105 (2012); T. Ribic, E. Assmann, A. Tóth, and K. Held, *ibid.* **90**, 165105 (2014).
[41] J. Kim, D. Casa, M. H. Upton, T. Gog, Y.-J. Kim, J. F. Mitchell, M. van Veenendaal, M. Daghofer, J. van den Brink, G. Khaliullin, and B. J. Kim, Phys. Rev. Lett. **108**, 177003 (2012).
[42] J. G. Vale, S. Boseggia, H. C. Walker, R. Springell, Z. Feng, E. C. Hunter, R. S. Perry, D. Prabhakaran, A. T. Boothroyd, S. P. Collins, H. M. Rønnow, and D. F. McMorrow, Phys. Rev. B **92**, 020406(R) (2015).
[43] F. Ye, S. Chi, B. C. Chakoumakos, J. A. Fernandez-Baca, T. Qi, and G. Cao, Phys. Rev. B **87**, 140406(R) (2013).
[44] S. Fujiyama, H. Ohsumi, T. Komesu, J. Matsuno, B. J. Kim, M. Takata, T. Arima, and H. Takagi, Phys. Rev. Lett. **108**, 247212 (2012).
[45] V. E. Dmitrienko, E. N. Ovchinnikova, S. P. Collins, G. Nisbet, G. Beutier, Y. O. Kvashnin, V. V. Mazurenko, A. I. Lichtenstein, and M. I. Katsnelson, Nat. Phys. **10**, 202 (2014).

[46] P. Liu, S. Khmelevskyi, B. Kim, M. Marsman, D. Li, X.-Q. Chen, D. D. Sarma, G. Kresse, and C. Franchini, Phys. Rev. B **92**, 054428 (2015).
[47] D. Singh and L. Nordström, *Planewaves, Pseudopotentials, and the LAPW Method* (Springer, New York, 2006); F. Bultmark, F. Cricchio, O. Grånäs, and L. Nordström, Phys. Rev. B **80**, 035121 (2009).
[48] M. Mochizuki and M. Imada, Phys. Rev. Lett. **91**, 167203 (2003).
[49] I. V. Solovyev, Phys. Rev. B **74**, 054412 (2006).
[50] L. Shekhtman, O. Entin-Wohlman, and A. Aharony, Phys. Rev. Lett. **69**, 836 (1992).
[51] T. Yildirim, A. B. Harris, A. Aharony, and O. Entin-Wohlman, Phys. Rev. B **52**, 10239 (1995).
[52] V. Yu. Irkhin and A. A. Katanin, Phys. Rev. B **60**, 2990 (1999).
[53] V. Yu. Irkhin and A. A. Katanin, Phys. Rev. B **55**, 12318 (1997).
[54] E. L. Nagaev, *Magnetics with Complex Magnetic Interactions* (Science, Moscow, 1988).
[55] A. A. Katanin and A. P. Kampf, Phys. Rev. B **66**, 100403(R) (2002).
[56] S. Chakravarty, B. I. Halperin, and D. R. Nelson, Phys. Rev. B **39**, 2344 (1989).